

# Trions in two-dimensional monolayers within the hyperspherical harmonics method. Application to transition metal dichalcogenides

Roman Ya. Kezerashvili<sup>1,2</sup>, Shalva M. Tsiklauri<sup>3</sup>, and Andrew Dublin<sup>1,2</sup>

<sup>1</sup>*New York City College of Technology, The City University of New York, USA*

<sup>2</sup>*The Graduate School and University Center, The City University of New York, USA*

<sup>3</sup>*Borough of Manhattan Community College, The City University of New York, USA*

(Dated: January 30, 2024)

We develop the theoretical formalism and study the formation of valley trions in two-dimensional monolayers within the framework of a nonrelativistic potential model using the method of hyperspherical harmonics (HH) in four-dimensional space. We present the solution of the three-body Schrödinger equation with the Rytova-Keldysh (RK) potential by expanding the wave function of a trion in terms of the HH.

We consider a long-range approximation when the RK potential is approximated by the Coulomb potential and a short-range limit when this potential is approximated by the logarithmic potential. In a diagonal approximation, the coupled system of differential equations for the hyperradial functions is decoupled in both limits. Our approach yields the analytical solution for binding energy and wave function of trions in the diagonal approximation for these two limiting cases: the Coulomb and logarithmic potentials. We obtain exact analytical expressions for eigenvalues and eigenfunctions for negatively and positively charged trions. The corresponding eigenvalues can be considered as the lower and upper limits for the trions binding energies.

We apply the proposed theoretical approach to describe trions in transition metal dichalcogenides (TMDC) and address the energy difference between the binding energies of  $X^-$  and  $X^+$  in TMDC. Results of numerical calculations for the ground state energies with the RK potential are in good agreement with similar calculations and in reasonable agreement with experimental measurements of trion binding energies.

## I. INTRODUCTION

In the last two decades, the condensed matter community has benefited from substantial progress in the understanding of excitons in band-gap two-dimensional (2D) semiconductors. Excitons are the most rudimentary bound quasiparticles formed by the electrostatic attraction between a positive valence-band hole and a conduction-band electron. Due to reduced dimensionality, diminished dielectric screening, and large charged carrier masses, the binding energies of excitons are quite large, with some reported energies as large as 0.5 eV [1].

The idea of the existence of a trion that is a bound state of an exciton with another charged carrier, which can either be an electron ( $X^-$  trion) or a hole ( $X^+$  trion) was first suggested by Lampert over 60 years ago [2]. This idea gave rise to many theoretical and experimental studies of trions in bulk materials and quantum-well systems from the 1960s to the 2000s. Only 35 years later, negatively charged trions were first observed in CdTe quantum-well system [3]. The positively charged trions were discovered three years later, in 1996 [4]. Theoretical calculations have shown that the binding energies of trions are very small in bulk materials [5], but they are substantially enhanced in structures of reduced dimensionality.

Since 2013, when trions were observed in two-dimensional MoS<sub>2</sub> monolayers [6], experimental and theoretical interests in trions in 2D materials have increased considerably. Reduced dielectric screening in 2D materials leads to greatly enhanced trion binding energies, whose signatures appear frequently in the optical spectra of monolayer transition metal dichalcogenides (TMDCs). TMDCs constitute a unique subgroup of crystalline, two-dimensional band-gap semiconductors whose compounds have a chemical formula MX<sub>2</sub>, where M and X denote a transition metal (Mo or W) and a chalcogenide (S, Se, or Te), respectively. Different experimental groups [6–27] observed and reported the signature of a trion in TMDCs formed from a hole in the first valence band and electrons originating predominantly from downwards curved conduction bands of the  $K$  and/or  $K'$  valleys.

Many studies have been carried out to calculate the binding energies of excitonic complexes in monolayer TMDCs (see reviews [28–32]). To study the physical properties of trions in 2D TMDC, one should know the wave function and the corresponding energy levels for a three-particle system. Theoretical studies of  $X^-$  and  $X^+$  trions [33–61] have integrated a wide variety of techniques and approaches, yielding impressively accurate results consistent with experimental data.

Within the framework of the variational method, a microscopic theory of an effective mass model of trions in TMDC monolayers was developed in Ref. [33]. The calculated binding energies are in good agreement with many-body computations based on the Bethe-Salpeter equation. Dark trions were predicted in Refs. [43, 44]. More

recently, trions have been studied using the variational method with trial wave functions constructed from 2D Slater-type orbitals [58]. Using the variational method, the trion binding energies and corresponding wave functions can be calculated efficiently with fairly good accuracy [27, 58].

The diffusion quantum Monte Carlo method was used for the Mott-Wannier model of trions in 2D semiconductors [35, 41, 42] and, most recently, for high-precision statistically exact quantum Monte Carlo calculations of the binding energies of 3D excitonic complexes [59]. Researchers have also made extensive use of the path-integral Monte Carlo method [36, 37] to study the effects of dielectric screening on trion binding energies, often incorporating stochastic variational techniques to improve ground-state energy estimates. Both the diffusion and the path-integral Monte Carlo methods have proven to be very effective in numerically solving the time-independent Schrödinger equation.

The stochastic variational method is applied to study the formation of trions within TMDC monolayers using a correlated Gaussian basis [38, 40] to investigate binding energies and their dependence on both the effective screening length and the electron-hole effective mass ratio. Stochastic variational methods have also been utilized to examine the effects of external magnetic fields and phonon recombination processes on excitonic binding energies [47]. Within the framework of the stochastic variational approach using the complex scaling and the stabilization method, it has been shown that there are narrow resonance states in two-dimensional three-particle systems of electrons and holes interacting via a screened Coulomb interaction [53].

In Ref. [39] the authors evaluate binding energies of  $X^\pm$  trions by mapping the three-body problem with three logarithmically interacting particles in two dimensions onto one particle in a three-dimensional potential treated with the boundary-matching-matrix method. The trion states are calculated by a direct diagonalization of the three-particle Hamiltonian within the Tamm–Dancoff approximation [54, 55].

Trions in TMDC monolayers have been investigated using both multi-band and single-band models, and the finite element method has been applied to both models [56]. In the framework of the multi-band model, the authors [56] constructed the excitonic Hamiltonian in the product base of the single-particle states at the conduction and valence band edges and solved the energy eigenvalue equation using the finite element as well as the stochastic variational [40, 62] methods.

The structural complexity of TMDCs gives rise to striking energetic properties. The periodicity of TMDC crystalline lattices permits the occupation of not only multiple charge and spin configurations, but also degenerate energy levels in the valence and conduction bands [63]. These bands are separated (in momentum space) by  $K$  and  $K'$  electron valleys [19]; the energy degeneracy at the valley boundary appears to be a direct result and manifestation of spin-orbit coupling and spin-splitting [21, 64, 65]. Researchers have posited that trion complexes can exist in different spin-valley configurations: the singlet and triplet states. The triplet state is more energetic due to long-range intervalley Coulomb attraction between the exciton and an additional conducting-band electron [64]. Substrate screening and doping are also believed to be significant contributors to these higher binding energies [19]. Interestingly, photoluminescence spectra in TMDC monolayers such as  $\text{WSe}_2$  suggest trion sensitivity to temperature [52, 64, 66]: as the temperature rises, the triplet states are believed to be more densely occupied than their singlet counterparts [64].

Much of our current understanding of exciton transitions and binding energies has emerged from optical spectroscopy [19, 21, 49, 65, 67]. Photoluminescence spectra and optical reflectivity measurements of  $\text{WSe}_2$  monolayers suggest a significant discrepancy between the binding energies of positive and negative trions [21]. In the effective mass approximation, it is hypothesized that short-range electron-hole and electron-electron Coulomb interactions [21, 57, 67] give rise to  $X^-$  fine-structure splitting in  $\text{WSe}_2$  monolayers, providing a possible explanation as to why the  $X^-$  binding energy is larger than that of the positive trion [21]. Similarly, optical red-shifts in the absorption spectra of  $\text{MoS}_2$  monolayers suggest that reductions in the exciton and trion binding energies are attributable, in large part, to a significant substrate-induced electric screening, substrate polarization, and doping, all of which are believed to diminish the Coulomb exchange interactions [19]. The theory of high-lying trions in 2D semiconductors with negative effective mass has been developed using the variational approach [60]. Authors have demonstrated the key role of the non-parabolicity of the high-lying conduction band dispersion in the formation of the bound exciton and trion states.

Excitonic systems are many-body systems, and the most systematic approach requires the use of quantum field theory. However, these excitonic systems can be well approximated and treated in the framework of few-body physics. There are different approaches to solving the three-body eigenvalue and eigenfunction problem in two dimensions for interacting electrons and holes [31]. The Faddeev equations and hyperspherical harmonic (HH) methods are commonly used in nuclear and atomic physics to solve the three-body problem in three-dimensional configuration or momentum spaces. Both methods are useful in studying three charged particles in a two-dimensional harmonic well and in calculating 2D trion energy levels, and both are implemented in Refs. [5, 45, 61, 68, 69].

In this paper, we develop a theoretical formalism for the three-body problem using the method of HH. The three-body problem is solved for one-layered systems within the effective mass approximation using the Rytova-Keldysh (RK) potential [70–72]. The HH method allows us to map the three-body problem in 2D configuration space onto a one-body problem in four-dimensional (4D) space. Separation of variables is invoked in the four-dimensional hyperspace to decouple the radial and angular dependence of the three-body wave function. Specifically, the wave

function is expanded in terms of the basis of angular eigenfunctions of the four-dimensional Laplace operator. Our approach yields the analytical solution for binding energies of trions in the diagonal approximation in two limiting cases - the Coulomb and logarithmic potentials. For the complete solution of the three-body Schrödinger equation with the effective two-dimensional screened potential [70, 71], we expand the wave functions of three bound particles in terms of the antisymmetrized hyperspherical harmonics. We then numerically solve the resulting coupled system of the second order differential equations.

This article has two foci and consists of two parts: i. the development of the technique to study trions in 2D monolayers in the framework of HH, and ii. the verification of this approach by its application to trions in TMDC. The article is organized as follows. In Sec. II, we present the theoretical approach and formalism to study Mott-Wannier trions in monolayer 2D semiconductors within the framework of the method of hyperspherical harmonics. We consider a non-relativistic potential model for three interacting particles and employ the three-body Schrödinger equation in the effective mass approximation. For the solution of the Schrödinger equation with the Rytova-Keldysh potential [70, 71], we expand the wave function of three bound particles in terms of the antisymmetrized hyperspherical harmonics, and obtain the corresponding system of coupled differential equations for the hyperradial functions. In Sec. III, the diagonal approximation is considered for the coupled differential equations for the hyperradial functions for two limiting cases of the RK potential: the Coulomb and logarithmic potentials. Our approach yields the analytical solutions for binding energies and wave functions of trions in the diagonal approximation for both the long-range Coulomb and short-range logarithmic potentials. In Sec. IV, we apply our approach to study trions in TMDC monolayers. We present and discuss results for the trions binding energies obtained by the numerical solution of the coupled differential equations for the RK potential and the results of calculations with the Coulomb and logarithmic potentials. Conclusions follow in Sec. V.

## II. THEORETICAL APPROACH AND FORMALISM

This Section provides an outline of the low-energy model that describes Mott-Wannier trions in 2D monolayers. We present a widely used screened electrostatic interaction between charged carriers in few-body complexes in two-dimensional materials and develop the hyperspherical harmonics formalism for trions in 2D monolayers.

### A. Charge-charge interaction

Within the effective mass approach, the non-relativistic Mott-Wannier trion Hamiltonian in a 2D configuration space reads

$$H = -\frac{\hbar^2}{2} \sum_{i=1}^3 \frac{1}{m_i} \nabla_i^2 + \sum_{i<j}^3 V_{ij}(|\mathbf{r}_i - \mathbf{r}_j|), \quad (1)$$

where  $m_i$  are the effective masses and  $\mathbf{r}_i$  are the  $i$ th particle Cartesian coordinates in 2D space. We assume only two types of charge carriers: electrons and holes, with the corresponding effective masses treated within the band effective mass approximation. In Eq. (1)  $V_{ij}(|\mathbf{r}_i - \mathbf{r}_j|)$  is the screened electromagnetic interaction between  $q_i$  and  $q_j$  point-like charges in 2D material, which was first derived in Ref. [70] and independently obtained by Keldysh [71]. The obtained spherical symmetry potential describes the interaction between two charged particles in a film of finite thickness under the intrinsic assumption that the screening can be quantified by the dielectric constant of the bulk material. In other words, the thickness of the film is assumed to be large with respect to the lattice constant. Thus, the dielectric constant is no longer a good parameter to quantify the macroscopic screening. In this case, the screening is best quantified by the 2D polarizability. In Ref. [72] the authors provide a strict 2D derivation of the macroscopic screening and obtain the screened charge-charge interaction, which has the same functional form as the potential [70, 71]. The effective charge-charge potential that describes the Coulomb interaction screened by the polarization of the electron orbitals in the 2D lattice reads

$$V_{ij}(r) = \frac{\pi k q_i q_j}{2\epsilon \rho_0} \left[ H_0 \left( \frac{r}{\rho_0} \right) - Y_0 \left( \frac{r}{\rho_0} \right) \right]. \quad (2)$$

In Eq. (2)  $r$  denotes the relative distance between the charge carriers, whose electric charges are  $q_i$  and  $q_j$ ,  $k = 9 \times 10^9 \text{ N}\cdot\text{m}^2/\text{C}^2$ ,  $\epsilon$  is the dielectric constant of the environment that is defined as  $\epsilon = (\epsilon_1 + \epsilon_2)/2$ , where  $\epsilon_1$  and  $\epsilon_2$  are the dielectric constants of two materials surrounding the TMDC layer,  $\rho_0$  is the screening length, and  $H_0 \left( \frac{r}{\rho_0} \right)$  and

$Y_0\left(\frac{r}{\rho_0}\right)$  are the Struve function and Bessel function of the second kind, respectively. In the case of a freestanding monolayer, in Ref. [72] it is shown that  $\rho_0 = 2\pi\chi$ , where  $\chi$  is the polarizability of the 2D material, which sets the boundary between two different behaviors of the potential due to a nonlocal macroscopic screening. Following Refs. [72–74] one can obtain that for the long-range, when  $r \gg \rho_0$ , the potential (2) has the three-dimensional bare Coulomb tail, while for the short-range, when  $r \ll \rho_0$ , it becomes a logarithmic potential like a potential of a point charge in two dimensions:

$$V_{ij}(r) = \begin{cases} \frac{kq_iq_j}{\epsilon r}, & \text{when } r \gg \rho_0, \text{ Coulomb potential,} \\ \frac{kq_iq_j}{\epsilon\rho_0} \left[ \ln\left(\frac{r}{2\rho_0}\right) + \gamma \right], & \text{when } r \ll \rho_0, \text{ Logarithmic potential,} \end{cases} \quad (3)$$

where  $\gamma$  is the Euler constant. Therefore, the potential (2) becomes the standard bare Coulomb potential for  $r \gg \rho_0$  and diverges logarithmically for  $r \ll \rho_0$ . A crossover between these two regimes takes place around distance  $\rho_0$ . From Eq. (3) one can conclude that increasing the screening length  $\rho_0$  leads to a decrease in the short-range interaction strength, which means that screening is more efficient in highly polarizable 2D materials, while the long-range interaction strength is unaffected. In Ref. [72], a very good approximation was introduced for the potential (2) in terms of elementary functions that is simpler to use in calculations, fairly precise in both limits, and accurate for all distances.

## B. Hyperspherical harmonics formalism

The Schrödinger equation for negative and positive trions with the interaction (2) reads

$$\left[ -\sum_{i=3}^3 \frac{\hbar^2}{2m_i} \nabla_i^2 + \sum_{i<j}^3 \frac{\pi k q_i q_j}{2\epsilon\rho_0} \left( H_0\left(\frac{|\mathbf{r}_i - \mathbf{r}_j|}{\rho_0}\right) - Y_0\left(\frac{|\mathbf{r}_i - \mathbf{r}_j|}{\rho_0}\right) \right) \right] \Psi(\mathbf{r}_1, \mathbf{r}_2, \mathbf{r}_3) = E\Psi(\mathbf{r}_1, \mathbf{r}_2, \mathbf{r}_3), \quad (4)$$

where  $\nabla_i^2$  is the 2D Laplace operator and  $E$  is the ground or excited states energy of the three-body system. At the first step one separates the center-of-mass (c.m.) motion from the relative motion of three particles through the transformation from the original Cartesian  $\mathbf{r}_1, \mathbf{r}_2, \mathbf{r}_3$  coordinates in 2D space to the set of mass-scaled 2D Jacobi coordinates shown in Fig. 1. We have three equivalent sets of Jacobi coordinates ( $i \neq j = 1, 2, 3$ ). For the partition  $i$ , the mass-scaled Jacobi coordinates are as follows

$$\begin{aligned} \mathbf{x}_i &= \sqrt{\frac{m_j m_k}{(m_j + m_k)\mu}} (\mathbf{r}_j - \mathbf{r}_k), \\ \mathbf{y}_i &= \sqrt{\frac{m_i (m_j + m_k)}{(m_i + m_j + m_k)\mu}} \left( \frac{m_j \mathbf{r}_j + m_k \mathbf{r}_k}{m_j + m_k} - \mathbf{r}_i \right), \quad i \neq j = 1, 2, 3, \end{aligned} \quad (5)$$

where

$$\mu = \sqrt{\frac{m_i m_j m_k}{m_i + m_j + m_k}} \quad (6)$$

is the three-particle effective mass. In Eqs. (5) the subscripts  $i, j$ , and  $k$  are a cyclic permutation of the particle numbers. After the transformation (5) that allows the separation of c.m. and relative motions of three particles with Hamiltonian (1), the Schrödinger equation for the relative motion of the three-body system reads

$$\left[ -\frac{\hbar^2}{2\mu} (\nabla_{x_i}^2 + \nabla_{y_i}^2) + V(x_1) + V(x_2) + V(x_3) \right] \Psi(\mathbf{x}_i, \mathbf{y}_i) = E\Psi(\mathbf{x}_i, \mathbf{y}_i). \quad (7)$$

In Eq. (7)  $V(x_i)$  is the interaction potential between two particles at the relative distance  $x_1, x_2$ , and  $x_3$ , respectively, where  $x_i$  is the modulus of the Jacobi vector  $\mathbf{x}_i$  (5), and (7) is written for any of set  $i = 1, 2, 3$  of the Jacobi coordinates (5). The orthogonal transformation between three equivalent sets of the Jacobi coordinates (see, for example, [75, 76]) simplifies calculations of matrix elements involving  $V(x_i)$  potentials. The total wave function  $\Psi(\mathbf{x}_i, \mathbf{y}_i)$  depends on one of the Jacobi coordinate sets  $\mathbf{x}_i, \mathbf{y}_i$ . Generally, the trion wave function  $\Psi(\mathbf{x}_i, \mathbf{y}_i)$  includes the electron-hole system spin function and the valence-band wave function [77].

For the solution of the Schrödinger equation (7) for the trion in 2D configuration space, we use the method of hyperspherical harmonics [78–81]. In the framework of this method, the problem of the motion of three particles in 2D space interacting via centrally symmetric potentials can be reduced to that of one particle in 4D space with an effective reduced mass (6). Therefore, instead of solving the three-body problem in 2D configuration space, we solve a one-body problem in a four-dimensional hyperspace. Thus, for our case, to solve Eq. (7) for a three-particle system in 2D space, we turn to hyperspherical coordinates and hyperspherical harmonics, which are the 4D generalizations of the familiar 3D spherical coordinates and spherical harmonics. The main idea of the HH method is the solution of the

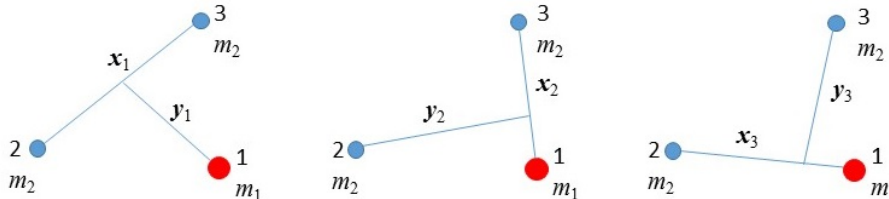


FIG. 1: (Color online) The partition trees of Jacobi coordinates for  $X^-$  trion.

Schrödinger equation (7) by separating the problem into two independent parts: an angular part and a radial part. This can be done by the expansion of the wave function of the trion  $\Psi(\mathbf{x}_i, \mathbf{y}_i)$  in terms of hyperspherical harmonics. The HH are the eigenfunctions of the angular part of the generalized Laplace operator in the 4D configuration space. The angular part of the problem is then solved analytically using elegant theorems involving hyperspherical harmonics in 4D space [79, 81]. For the radial part, we obtain the system of coupled one-dimensional differential equations for the hyperradial functions that can be solved numerically. In a diagonal approximation, for a particular form of interparticle interactions, the system of coupled differential equations can be solved analytically.

Due to the spherical symmetry of  $V(x_i)$  we employ hyperspherical coordinates in 4D configuration space to obtain a solution of Eq. (7) for the trion. This allows us to separate the radial and angular variables and reduce Eq. (7) for the system of coupled one-dimensional radial equations. We introduce in 4D space the hyperradius  $\rho = \sqrt{x_i^2 + y_i^2}$  and a set of three angles  $\Omega_i \equiv (\alpha_i, \varphi_{x_i}, \varphi_{y_i})$ , where  $\varphi_{x_i}$  and  $\varphi_{y_i}$  are the polar angles for 2D Jacobi vectors  $\mathbf{x}_i$  and  $\mathbf{y}_j$ , respectively, and  $\alpha_i$  is an angle defined as  $x_i = \rho \cos \alpha_i$ ,  $y_i = \rho \sin \alpha_i$ . After transforming from the Jacobi coordinates  $\mathbf{x}_i$  and  $\mathbf{y}_i$  to the hyperspherical coordinates  $\rho$  and  $\Omega_i$ , and using the familiar expression for the Laplacian operator in the 4D configuration space [79, 81], Eq. (7) can be rewritten as

$$\left[ -\frac{\hbar^2}{2\mu} \left( \frac{\partial^2}{\partial \rho^2} + \frac{3}{\rho} \frac{\partial}{\partial \rho} - \frac{\widehat{K}^2(\Omega_i)}{\rho^2} \right) + \sum_{j=1}^3 V(\rho \cos \alpha_j) - E \right] \Psi(\rho, \Omega_i) = 0, \quad (8)$$

where  $\widehat{K}^2(\Omega_i)$  is the angular part of the generalized Laplace operator in 4D configuration space known as the grand-angular momentum operator [78, 79, 81]

$$\begin{aligned} \widehat{K}^2(\Omega_i) &= \frac{d^2}{d\alpha_i^2} + 2 \cot 2\alpha_i \frac{d}{d\alpha_i} - \frac{\widehat{l}^2(\varphi_{x_i})}{\cos \alpha_i} - \frac{\widehat{l}^2(\varphi_{y_i})}{\sin \alpha_i}, \\ \widehat{l}(\varphi_{x_i}) &= -i \frac{d}{d\varphi_{x_i}}, \quad \widehat{l}(\varphi_{y_i}) = -i \frac{d}{d\varphi_{y_i}}, \quad \Omega_i \equiv (\alpha_i, \widehat{\mathbf{x}}_i, \widehat{\mathbf{y}}_i). \end{aligned} \quad (9)$$

We shall seek the common eigenfunctions of the operator  $\widehat{K}^2(\Omega_i)$  and (8). One can expand the wave function of the trion  $\Psi(\rho, \Omega_i)$  in terms of the HH that are the eigenfunctions of the operator  $\widehat{K}^2$ :

$$\widehat{K}^2(\Omega) \Phi_K^{l_x m_x l_y m_y}(\Omega) = K(K+2) \Phi_K^{l_x m_x l_y m_y}(\Omega). \quad (10)$$

The grand-angular momentum  $K = 2n + l_x + l_y$ , where  $l_x$  and  $l_y$  are angular momenta corresponding to the Jacobi coordinates  $\mathbf{x}$  and  $\mathbf{y}$ , respectively, and  $n \geq 0$  is an integer number. The eigenfunctions  $\Phi_K^{l_x m_x l_y m_y}(\Omega)$  present a complete set of the orthonormal basis. The function  $\Phi_K^{l_x l_y LM}(\Omega) \equiv \Phi_{K\lambda}^L(\Omega)$  (here and below we use the short-hand notation  $\lambda \equiv \{l_x, l_y\}$ ) with the total orbital angular momentum of the trion  $L$  and its projection  $M$ , is a linear combination of HH  $\Phi_K^{l_x m_x l_y m_y}(\Omega)$ , given by:

$$\Phi_{K\lambda}^L(\Omega) = \sum_{m_x m_y} \langle l_x m_x l_y m_y | LM \rangle \Phi_K^{l_x m_x l_y m_y}(\Omega), \quad (11)$$

where  $\langle l_x m_x l_y m_y | LM \rangle$  are the Clebsch–Gordan coefficients. The equation (11) is valid for each partition  $i$  for the Jacobi coordinates. The  $\Phi_{K\lambda}^L(\Omega)$  are also the eigenfunctions of the operator  $\widehat{K}^2$ . The expansion of  $\Psi(\rho, \Omega_i)$  in terms of  $\Phi_{K\lambda}^L(\Omega)$  reads

$$\Psi(\rho, \Omega_i) = \rho^{-3/2} \sum_{\kappa\lambda} u_{K\lambda}^L(\rho) \Phi_{K\lambda}^L(\Omega). \quad (12)$$

In Eq. (12)  $u_{K\lambda}^L(\rho)$  are the hyperradial functions for the trion state with the total orbital angular momentum  $L$ . By substituting (12) into (8), then multiplying on the left by  $\Phi_{K\lambda}^{L*}(\Omega_i)$  and integrating over the hyperangles, we separate the radial and angular variables and obtain the set of coupled differential equations for the hyperradial functions  $u_{K\lambda}^L(\rho)$ :

$$\left[ \frac{d^2}{d\rho^2} - \frac{(K+1)^2 - 1/4}{\rho^2} + \kappa^2 \right] u_{K\lambda}^L(\rho) = \frac{2\mu}{\hbar^2} \sum_{\kappa'\lambda'} \mathcal{W}_{K\lambda K'\lambda'}^L(\rho) u_{K'\lambda'}^L(\rho). \quad (13)$$

In Eq. (13)  $\kappa^2 = 2\mu B/\hbar^2$ , where  $B$  is the trion binding energy, and the effective potential energy  $\mathcal{W}_{K\lambda K'\lambda'}^L(\rho)$  is

$$\mathcal{W}_{K\lambda K'\lambda'}^L(\rho) = \int \Phi_{K\lambda}^{L*}(\Omega_1) \sum_{j=1}^3 V(\rho \cos \alpha_j) \Phi_{K'\lambda'}^L(\Omega_1) d\Omega_1. \quad (14)$$

The coupled system of equations (13) describes the motion of one particle in the centrally symmetric coupling effective field (14). The coupling effective interaction (14) is defined via the RK potential (2). Substituting (2) into Eq. (14), one obtains

$$\begin{aligned} \mathcal{W}_{K\lambda K'\lambda'}^L(\rho) = & \frac{\pi k e^2}{2\epsilon\rho_0} \left\{ \int \Phi_{K\lambda}^{L*}(\Omega_1) \left[ H_0\left(\frac{x_1}{b_j\rho_0}\right) - Y_0\left(\frac{x_1}{b_j\rho_0}\right) \right] \Phi_{K'\lambda'}^L(\Omega_1) d\Omega_1 - \right. \\ & \int \Phi_{K\lambda}^{L*}(\Omega_1) \left[ H_0\left(\frac{x_2}{b_j\rho_0}\right) - Y_0\left(\frac{x_2}{b_j\rho_0}\right) \right] \Phi_{K'\lambda'}^L(\Omega_1) d\Omega_1 - \\ & \left. \int \Phi_{K\lambda}^{L*}(\Omega_1) \left[ H_0\left(\frac{x_3}{b_j\rho_0}\right) - Y_0\left(\frac{x_3}{b_j\rho_0}\right) \right] \Phi_{K'\lambda'}^L(\Omega_1) d\Omega_1 \right\}. \end{aligned} \quad (15)$$

where

$$b_1 = \sqrt{\frac{m_2 m_3}{(m_2 + m_3)\mu}}, \quad b_2 = \sqrt{\frac{m_1 m_3}{(m_1 + m_3)\mu}}, \quad b_3 = \sqrt{\frac{m_1 m_2}{(m_1 + m_2)\mu}}, \quad (16)$$

$$x_1 = \rho \cos \alpha_1, \quad x_2 = \rho \cos \alpha_2, \quad x_3 = \rho \cos \alpha_3; \quad d\Omega_i = \cos \alpha_i \sin \alpha_i d\alpha_i d\varphi_{x_i} d\varphi_{y_i}. \quad (17)$$

The  $X^-$  and  $X^+$  trions have two identical particles, two electrons and two holes, respectively. Below we always assume that indices 2 and 3 identify the identical particles. The total wave function of the system is antisymmetric with respect to the permutation of the identical particles. Calculation of matrix elements  $\mathcal{W}_{K\lambda K'\lambda'}(\rho)$  of the two-body  $V(\rho \cos \alpha_j)$  interactions in the hyperspherical harmonics expansion method for a three-body system is greatly simplified by using the HH basis states appropriate for the partition corresponding to the interacting pair. There are three terms in the integral (15). From these three terms, it is relatively easy to calculate only one term whose index of the  $x_i$  coincides with the index of the set of angles on which the hyperspherical functions  $\Phi_{K'\lambda'}^L(\Omega_i)$  depend. In this case the evaluation of the integrals by the polar angles for the Jacobi vectors  $\mathbf{x}_i$  and  $\mathbf{y}_i$  can be done analytically in a complete form using the properties of hyperspherical harmonics. Direct calculations of the other two terms are a challenging task. To simplify the calculations, it is convenient to use a unitary transformation that involves the Reynal-Revai coefficients (RRC) [82], which are the transformation coefficients between the HH bases corresponding to the two partitions and give the relationship between the HH defined on the two different sets of Jacobi coordinates. The use of RRC becomes particularly essential for the numerical solution of the three-body Schrödinger equation where the two-body potentials do not allow analytical integration by the angles. The Reynal-Revai unitary transformation

between different bases of HH functions (transformation from the HH basis for the partition  $k$  to the HH basis for the partition  $i$ ) has the following form

$$\Phi_{K\lambda_i}^L(\Omega_i) = \sum_{\lambda_k} \langle \lambda_k | \lambda_i \rangle_{KL} \Phi_{K\lambda_k}^L(\Omega_k), \quad (18)$$

where  $\langle \lambda_k | \lambda_i \rangle_{KL} \equiv \langle l_{x_k} l_{y_k} | l_{x_i} l_{y_i} \rangle_{KL}$  are Reynal-Revai coefficients. The Reynal-Revai unitary transformation does not change the global momentum  $K$  and the total angular momentum  $L$  of the three-particle system. By using the unitary transformation (18), Eq. (15) can be written in the following form

$$W_{KK'\lambda\lambda'}^L(\rho) = \left( \mathcal{K}_{K\lambda K'\lambda'}^{(1)} - \sum_{\lambda_k \lambda'_k} \langle \lambda_k | \lambda_i \rangle_{KL} \langle \lambda'_k | \lambda_i \rangle_{K'L} \mathcal{K}_{K\lambda K'\lambda'}^{(2)} - \sum_{\lambda_j \lambda'_j} \langle \lambda_j | \lambda_i \rangle_{KL} \langle \lambda'_j | \lambda_i \rangle_{K'L} \mathcal{K}_{K\lambda K'\lambda'}^{(3)} \right), \quad (19)$$

where

$$\mathcal{K}_{K\lambda K'\lambda'}^{(i)} = \frac{\pi k e^2}{2\epsilon \rho_0} \int \Phi_{K\lambda}^{L*}(\Omega_i) \left[ H_0\left(\frac{\rho \cos \alpha_i}{b_i \rho_0}\right) - Y_0\left(\frac{\rho \cos \alpha_i}{b_i \rho_0}\right) \right] \Phi_{K'\lambda'}^L(\Omega_i) \cos \alpha_i \sin \alpha_i d\alpha_i d\varphi_{x_i} d\varphi_{y_i}, \quad i = 1, 2, 3. \quad (20)$$

Using the matrix elements of the effective potential energies (20), one can solve the coupled differential equations (13) numerically. However, one can obtain analytical solutions for the trion in the diagonal approximation for a long- and short-range approximations of the 2D screened charge-charge interactions given by Eq. (3). The results of the approximate analytical and numerical solutions of Eq. (13) are presented in the next sections.

### III. APPROXIMATE ANALYTICAL SOLUTIONS

The finding of the binding energy and wave function for a trion requires the solution of the system of equations (13) coupled via the potential energy (19). Many calculations in atomic and nuclear physics that have been made within the framework of the HH method use approximations for the solution of the coupled differential equations for the hyperradial functions. In this Section, we obtain analytical solutions for the trion in the diagonal approximation for both long- and short-range approximations of the 2D screened charge-charge interaction. In the diagonal approximation, the coupled differential equations (13) will be decoupled.

Let us consider the solution of Eq. (13) with the effective potential energy (19) for the long- and short-range interactions (3). The matrix elements (19) for a central potential when  $K = K'$  and  $\lambda = \lambda'$  (diagonal matrix elements) are much larger than non-diagonal matrix elements and make the main contribution to the binding energy. From the other side, if one neglects the non-diagonal matrix elements, the differential equations (13) will be decoupled. It is easier to solve decoupled equations numerically with much less computational complexity. Moreover, for some central potentials, the diagonal approximation even allows to obtain an analytical solution for the decoupled equations. Below we obtain analytical solutions of Eq. (13) in the limits  $r \gg \rho_0$  and  $r \ll \rho_0$  for the potentials (3) in the diagonal approximation.

#### A. Long-range limit: $r \gg \rho_0$

Consider the long range  $r \gg \rho_0$  limit when the Keldysh potential can be approximated by the Coulomb potential (3). In this case, the effective potential energy (14) can be written as

$$\mathcal{W}_{K\lambda K'\lambda'}^L(\rho) = k \int \Phi_{K\lambda}^{L*}(\Omega_1) \left( \frac{b_1}{x_1} - \frac{b_2}{x_2} - \frac{b_3}{x_3} \right) \Phi_{K'\lambda'}^L(\Omega_1) d\Omega_1. \quad (21)$$

In Eq. (21)  $b_1, b_2, b_3$  and  $x_1, x_2, x_3$  are defined in Eqs. (16) and (17), respectively. By using the Reynal-Revai unitary transformation (18) for the fixed global momentum  $K$  and the total angular momentum  $L$ , as well as Eq. (17), one can rewrite (21) in the following form

$$\mathcal{W}_{K\lambda K'\lambda'}^L(\rho) = \frac{\mathcal{G}_{K\lambda K'\lambda'}^L}{\rho}, \quad (22)$$

where

$$\mathcal{G}_{K\lambda K'\lambda'}^L = ke^2 \left( b_1 \mathcal{C}_{K\lambda K'\lambda'}^{(1)} - b_2 \sum_{\lambda_k \lambda'_k} \langle \lambda_k | \lambda_i \rangle_{KL} \langle \lambda'_k | \lambda_i \rangle_{K'L} \mathcal{C}_{K\lambda K'\lambda'}^{(2)} - b_3 \sum_{\lambda_j \lambda'_j} \langle \lambda_j | \lambda_i \rangle_{KL} \langle \lambda'_j | \lambda_i \rangle_{K'L} \mathcal{C}_{K\lambda K'\lambda'}^{(3)} \right), \quad (23)$$

and

$$\mathcal{C}_{K\lambda K'\lambda'}^{(i)} = \int \Phi_{K\lambda}^{L*}(\Omega_i) \left( \frac{1}{\cos \alpha_i} \right) \Phi_{K'\lambda'}^L(\Omega_i) d\Omega_i, \quad i = 1, 2, 3. \quad (24)$$

All integrals (24) can be evaluated in a closed analytic form using the properties of HH [78, 79, 81] and the corresponding expressions are presented in Appendix A.

Consider the diagonal approximation when  $K = K'$ ,  $\lambda = \lambda'$ . The latter leads to the reduction of the system of equations (13) to a simpler form. In this case, the system of equations (13) will be decoupled and reduced to the following differential equation:

$$\left[ \frac{d^2}{d\rho^2} - \frac{(K+1)^2 - 1/4}{\rho^2} + \kappa^2 \right] u_{K\lambda}^L(\rho) = \frac{2\mu}{\hbar^2} \frac{\mathcal{G}_{K\lambda K\lambda}^L}{\rho} u_{K\lambda}^L(\rho). \quad (25)$$

Eq. (25) has the same dependence on the variable  $\rho$  as the 3D radial Schrödinger equation for a hydrogen atom. Following the standard procedure for the solution of the radial Schrödinger equation for a hydrogen atom in 3D space [83], which was generalized for 2D space [84–87], one can solve Eq. (25) analytically and obtain eigenenergies and eigenfunctions

$$E = -\frac{\mu}{\hbar^2} \frac{(\mathcal{G}_{K\lambda K\lambda}^L)^2}{2(N+K+3/2)^2}, \quad (26)$$

$$u_K(\rho) = C_K \rho^{K+3/2} \exp(-\kappa\rho) L_N^{2K+2}(2\kappa\rho) \quad (27)$$

where  $N = 1, 2, \dots$ ,  $L_N^{2K+2}$  is a Laguerre polynomial,  $C_K$  is a normalization constant and  $\mathcal{G}_{K\lambda K\lambda}^L$  are defined by (23) when  $K = K'$ ,  $\lambda = \lambda'$ . In this case (23) becomes much more compact.

### B. Short-range limit: $r \ll \rho_0$

Now let us consider a short-range limit  $r \ll \rho_0$  in which the RK potential can be approximated by the logarithmic potential (3). The logarithmic potential is very widely used as a quark confinement potential in high energy physics. The solution of the Schrödinger equation with the logarithmic potential is a very complex problem. There are only almost complete solutions of the Schrödinger equation for the logarithmic potential [88–90]. In Ref. [39] a remarkable solution for the trion with a logarithmic potential was obtained, but only for the case, where the full Rytova-Keldysh effective potential is replaced with a completely logarithmic form. Below, we consider the logarithmic potential, which has a shift due to the asymptotic approximation of the RK potential at  $r \ll \rho_0$ , as it is seen from Eq. (3). Using the corresponding Jacobi coordinates, the effective potential energy (14) can be written as

$$\mathcal{W}_{K\lambda K'\lambda'}^L(\rho) = \frac{ke^2}{\epsilon\rho_0} \int \Phi_{K\lambda}^{L*}(\Omega_1) \left( \ln \frac{x_1}{2b_1\rho_0} + \gamma \right) - \left( \ln \frac{x_2}{2b_2\rho_0} + \gamma \right) - \left( \ln \frac{x_3}{2b_3\rho_0} + \gamma \right) \Phi_{K'\lambda'}^L(\Omega_1) d\Omega_1, \quad (28)$$

where  $b_1, b_2, b_3$ , and  $x_1, x_2, x_3$  are defined in Eqs. (16) and (17), respectively. The effective potential energy can be evaluated by employing the Reynal-Revai unitary transformation. As a result, we have

$$\mathcal{W}_{K\lambda K'\lambda'}^L(\rho) = -\frac{ke^2}{\epsilon\rho_0} \ln \frac{\rho}{\rho_0} + \mathcal{B}_{123} + \mathcal{J}_{K\lambda K'\lambda'}^L, \quad (29)$$



where

$$\mathcal{B}_{123} = \frac{ke^2}{\epsilon\rho_0} \left( \ln \frac{2b_2b_3}{b_1} - \gamma \right), \quad (30)$$

$$\mathcal{J}_{K\lambda K'\lambda'}^L = \frac{ke^2}{\epsilon\rho_0} \left( \mathcal{L}_{K\lambda K'\lambda'}^{(1)} - \sum_{\lambda_k \lambda'_k} \langle \lambda_k | \lambda_i \rangle_{KL} \langle \lambda'_k | \lambda_i \rangle_{K'L} \mathcal{L}_{K\lambda K'\lambda'}^{(2)} - \sum_{\lambda_j \lambda'_j} \langle \lambda_j | \lambda_i \rangle_{KL} \langle \lambda'_j | \lambda_i \rangle_{K'L} \mathcal{L}_{K\lambda K'\lambda'}^{(3)} \right). \quad (31)$$

In Eq. (31)  $\mathcal{L}_{K\lambda K'\lambda'}^{(i)}$  is defined as

$$\mathcal{L}_{K\lambda K'\lambda'}^{(i)} = \int \Phi_{K\lambda}^{L*}(\Omega_i) \ln \cos \alpha_i \Phi_{K'\lambda'}^L(\Omega_i) d\Omega_i, \quad i = 1, 2, 3. \quad (32)$$

and can be found in a closed analytic form for any  $K\lambda K'\lambda'$  set and corresponding expression for (32) is presented in Appendix B.

Substituting (29) into Eq. (13), one obtains the coupled differential equations for the hyperradial functions  $u_{K\lambda}(\rho)$  for the trion in the asymptotic region  $r \ll \rho_0$ . The latter system of equations can be written in a diagonal approximation when  $K = K'$  and  $\lambda = \lambda'$ , leading to the following equation

$$\left[ \frac{d^2}{d\rho^2} - \frac{(K+1)^2 - 1/4}{\rho^2} + \kappa^2 \right] u_{K\lambda}^L(\rho) = \frac{2\mu}{\hbar^2} \left( -\frac{ke^2}{\epsilon\rho_0} \ln \frac{\rho}{\rho_0} + \mathcal{B}_{123} + \mathcal{J}_{K\lambda K\lambda}^L \right) u_{K\lambda}^L(\rho). \quad (33)$$

Equation (33) can be rewritten in the following form

$$\left[ \frac{d^2}{d\rho^2} + \left( \alpha - \beta \ln \rho - \frac{(K+1)^2 - 1/4}{\rho^2} \right) \right] u_{K\lambda}^L(\rho) = 0. \quad (34)$$

Here we have defined

$$\alpha = \kappa^2 (2\mu B / \hbar^2) + \frac{2\mu}{\hbar^2} \left( \frac{ke^2}{\epsilon\rho_0} \ln \rho_0 - \mathcal{B}_{123} - \mathcal{J}_{K\lambda K\lambda} \right), \quad \beta = \frac{2\mu}{\hbar^2} \frac{ke^2}{\epsilon\rho_0}. \quad (35)$$

Note that  $\mathcal{J}_{K\lambda K\lambda}^L$  is defined in Eq. (29) when  $K = K'$ ,  $\lambda = \lambda'$ . In this case Eq. (29) becomes much more compact.

One can find the approximate analytical solution of Eq. (34) by rescaling the variable  $\rho$  and introducing a new function that allows us to reduce Eq. (34) to the known Weber's equation [91]. The reduction of Eq. (34) to the Weber's equation is given in Appendix C. The solution of this equation in a first approximation is simply the parabolic cylinder functions  $D_n$ . The eigenvalues that correspond to these eigenfunctions are

$$E = -\frac{ke^2}{\epsilon\rho_0} \ln \rho_0 + \mathcal{B}_{123} + \mathcal{J}_{K\lambda K\lambda} + \frac{ke^2}{\epsilon\rho_0} \left\{ 1 + \ln \left[ \frac{[n + 1/2 + \sqrt{(n + 1/2)^2 + (K + 2)^2/16}]^2}{\beta} \right] \right\}, \quad n = 0, 1, 2, \dots \quad (36)$$

#### IV. APPLICATION TO TMDCs: RESULTS AND DISCUSSION

We apply the present theoretical approach for calculations of the trion binding energies in the following TMDC monolayers: MoS<sub>2</sub>, MoSe<sub>2</sub>, WS<sub>2</sub>, and WSe<sub>2</sub>. A schematic representation of a trion in freestanding, supported, and encapsulated TMDC monolayers is given in Fig. 2. The form of the trion wave function (12) is most general, not restricted to any particular mass ratio of electrons and holes, and describes the three-particle relative motion. However, two from three particles constituting a positive or a negatively trion in the monolayer plane must be identical, as shown in Fig. 2. Two identical particles must have different spin and/or valley indices and a trion is formed by the singlet or triplet excitons. Therefore, it can be in either a single or triplet state.

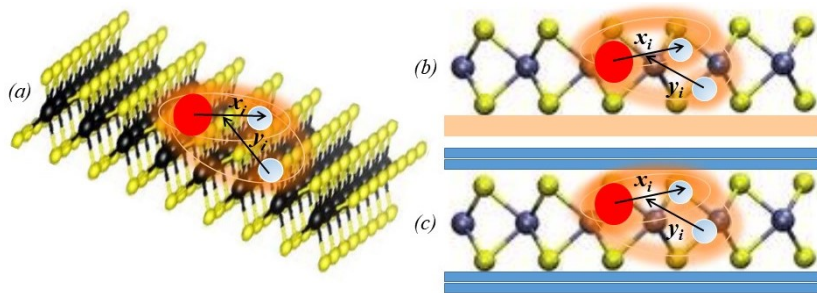


FIG. 2: (Color online) Schematic representation of the trion in (a) freestanding, (b) supported and (c) encapsulated TMDC monolayer.  $x_i$  and  $y_i$  are Jacobi coordinates for the partition  $i$ .

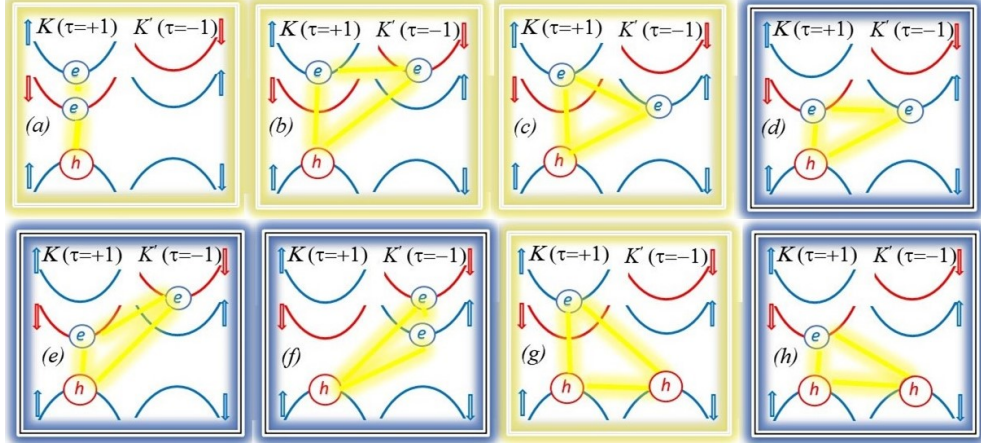
### A. Intravalley and intervalley trions

Trions play an important role in the fundamental valley dynamics in emerging two-dimensional semiconductor materials. Trions properties in 2D TMDC are associated with their spin and valley degrees of freedom. The lack of inversion symmetry, together with a strong spin-orbit coupling, leads to a large valence band splitting in monolayer TMDCs [77]. This splitting lifts the spin degeneracy of both electron and hole states in the  $K$  and  $K'$  valleys, enabling the excitation of carriers with various combinations of spin and valley indices. The valley degree of freedom has been vastly explored in monolayers of molybdenum- and tungsten-based dichalcogenides using helicity-resolved photoluminescence, time-resolved photoluminescence, reflectance spectra and the time-resolved Kerr rotation technique [8, 13, 93–102]. The absolute minima of the conduction and absolute maxima of the valence bands in TMDC monolayers are at two non-equivalent hexagonal Brillouin zone corners of the  $K$  and  $K'$  valleys. The inversion symmetry breaking with the spin-orbit interaction leads to the carrier spin and valley coupling so that the circular polarization of the absorbed or emitted photon can be directly associated with a specific valley,  $K$  or  $K'$  [77, 96]. This valley contrasting optical selection rules allow one to address and manipulate the valley index. Experimental studies [93, 94] show that each of the valleys can be excited by radiation of given helicity. Having a valley index  $\tau$  in addition to spin, one can distinguish between two types of trions: the intravalley and intervalley trions. Our theoretical approach allows consideration of this degree of freedom. For intravalley trions  $\tau_1 = \tau_2$ , while for intervalley trions  $\tau_1 \neq \tau_2$ . A symmetry analysis of the different  $X^-$  and  $X^+$  trion states, classified by the valley configurations as well as the spin configuration, is performed [21, 28, 39, 52]. Depending on the spin configuration of the electron-hole pairs, intravalley excitons of TMDC monolayers can be either optically bright or dark. The analysis [21, 28, 52, 102] shows that the negative and positive trions can be optically bright or dark. Experimental studies [23, 103] have revealed evidence of dark trions in monolayer  $\text{WSe}_2$  under a strong in-plane magnetic field.

The atomic spin-orbit interaction in TMDC introduces large spin-orbit splitting of the valence band, so that the low-energy trions involve only the lowest hole states [104, 105], because in the  $K$  and  $K'$  valleys, the spin-orbit splitting of the valence band is much larger than that of the conduction band [77]. The developed theoretical formalism allows us to consider a three-band model, consisting of a higher spin branch of the valence band and both spin branches of the conduction band. We consider only one possible hole spin state at the topmost valence band in a given valley [104, 105]: spin up in the  $K$  valley and spin down in the  $K'$  valley. However, because the spin-orbit interaction for electrons is much smaller than the trion binding energy, one should take for each electron four states coming from the spin and valley degeneracy. The negative trions can be bright or dark. When the electron and hole come from bands with the same electron spin, their recombination emits light. This is a bright exciton. When the electron is in the bottom spin-orbit split state, the spin of the electron and hole mismatch. The spin mismatch strongly suppresses the radiative recombination of the electron and hole. This is a dark exciton. In finite charge density, bright and dark excitons can interact with the Fermi sea to form bright and dark trions. Dark trions were predicted in Refs. [43, 44]. The intravalley  $X^-$  trion in the spin-singlet state, with both electrons and a hole in the same valley, is a bright spin singlet trion (Fig. 3a). The intervalley trions with electrons in two different valleys can be bright (Fig. 3b and 3c) or dark (Fig. 3d, e, f), depending on the spin of the electrons state in the different valleys. Thus, the intravalley  $X^-$  trion is in a spin singlet state, while the intervalley  $X^-$  trion can be in a spin singlet or spin triplet state. Consequently,  $X^-$  can be of both spin-forbidden and momentum-forbidden types. The most intriguing feature is that in cross-circularly polarized experiments, trions created in the  $K$  valley in the singlet state (Fig. 3a) are converted to intervalley singlet trions with an electron in the  $K'$  valley (Fig. 3c) via the spin flip and electron-hole exchange interaction [18].

The positive trion is formed of two holes occupying the topmost valence band sub bands and the electron in conduction band sub bands is always the intervalley trion.  $X^+$  is a bright trion when the spin orientation of the electron and hole is the same (Fig. 3g). Otherwise,  $X^+$  is dark trion (Fig. 3h).

FIG. 3: (Color online) Schematic illustration of WSe<sub>2</sub> low-energy band structure and the spin-valley configurations of the constituent charge carriers. The topmost spin-subband for the valence band and the lower and upper spin-orbit splitting conduction band are shown. Arrows denote bands with up (down) spin. The hole has the opposite spin of the valence electron [92]. Light and dark rectangles indicate the bright and dark trions, respectively. (a), (b), (c), (d), and (e) correspond to  $X^-$  trions. (g) and (h) correspond to  $X^+$  trions. The bright trions emit circularly polarized light in the out-of-monolayer plane direction, while the dark trions emit vertically polarized light in the in-monolayer plane direction [23]. Lines indicate interaction between three charged particles. The remaining configurations are the time reversal of those shown in the figure.



The  $X^-$  trion consists of two electrons of opposite spin in the two conduction bands as well as one hole in the topmost valence band. Consequently, the intravalley  $X^-$  trion ( $\tau_1 = \tau_2$ ) must exist in the spin-singlet state, whereas the intervalley  $X^-$  trion ( $\tau_1 \neq \tau_2$ ) can exist in either the singlet or triplet states. Intravalley  $X^-$  trions have been shown to be optically bright (radiative), provided that the spins of a paired electron and hole differ. In contrast, intervalley  $X^-$  trions in TMDC monolayers such as the molybdenum- and tungsten-based dichalcogenides have given rise to both optically bright and dark spin-valley configurations; the resulting optical configuration is contingent on the lone electron's spin as well as its occupation of either the outermost or innermost conduction bands in the  $K'$  valley [23, 28]. It is important to note that for intravalley  $X^-$  trions with identical electron masses, the wave function antisymmetrization is performed with respect to the spin states of the two electrons. However, if the two intravalley electrons have unequal masses, calculations must be performed in the context of a three-body problem.

In contrast, the  $X^+$  trion, consists of two holes in the outermost valence band of the  $K-$  and  $K'$ -valleys as well as an unpaired electron in either the innermost or outermost  $K$ -valley conduction sub-bands. By the Pauli exclusion principle, the  $X^+$  trion can only exist in the intervalley configuration. It is important to note that for intervalley  $X^+$  trions, the wave function's antisymmetrization is performed with respect to the spin states of the two holes that have identical masses. Interestingly, spectroscopic measurements in MoS<sub>2</sub> and MoSe<sub>2</sub> monolayers confirm the presence of  $X^+$  spin-splitting in the innermost and outermost  $K$ -valley conduction sub-bands, giving rise to both optically bright and dark configurations. This is in stark contrast to the  $X^+$  trions in monolayers such as WS<sub>2</sub> and WSe<sub>2</sub>, neither of which permits such overlapping of the  $K$ -valley conduction sub-bands. Such overlapping, which is uniquely characteristic of positive and negative trions in MoS<sub>2</sub> and MoSe<sub>2</sub>, is attributed to differences in the effective masses of the conduction sub-bands caused by the spin-orbit coupling [23, 28].

### B. Binding energies in short- and long-range limits

To calculate trion binding energies, one should solve the system of coupled differential equations (13) with the RK potential. The latter system includes the electron and hole effective masses, a screening distance, and dielectric constants of a supported or encapsulated material. In our theoretical approach, all these characteristics are the input parameters. In this sense, our approach has no fitting parameters. In our calculations, we use the necessary parameters for the trions that were calculated from first principles. The resulting binding energies of positive or negative trions in the monolayer have a parametric dependence on the screening distance  $\rho_0$  and the electron,  $m_e$ , and hole,  $m_h$ , effective masses. In our calculations we use the effective masses from Ref. [1] that are extracted from the low energy band structure obtained in *ab initio* density functional theory calculations to describe the dispersion of the valence and conduction bands at their extrema. The screening length was calculated using the polarizability  $\chi$  for TMDCs given in Ref. [33, 104].

Before presenting the results for the trion binding energies obtained by the numerical solution of the system of equations (13) with the potential (2), we calculate the binding energies in both the long- and short-range limits within the diagonal approximation for freestanding TMDC monolayers. Calculations are performed using analytical expressions (26) and (36), respectively, for the single state intravalley  $X^-$  trions formed in the  $K$  valley, and are shown in Table I. For simplicity, in the binding energy calculation, we consider the contribution of the term  $K = 0$ . The latter leads to the reduction of the equations in the diagonal approximation to only a single equation.

TABLE I:  $X^-$  trion binding energies in meV in the short  $r \ll \rho_0$  and long  $r \gg \rho_0$  range limits. Calculations are performed in the diagonal approximation, when  $K = 0$  for the state  $(S, L) = (1/2, 0)$  and with the electron and hole effective masses from Ref. [1].  $m_0$  is the free electron mass. The calculations are performed for freestanding monolayers. The data [39] are estimated using Fig. 1 from this work for the ratio  $m_e/m_h$  given in the Table.

	Input parameters			Theory, $r \ll \rho$		Theory, $r \gg \rho$	Experiment
	$m_e/m_0$	$m_h/m_0$	$\rho_0, \text{\AA}$	This work	[39]	This work	
MoS <sub>2</sub>	0.350	0.428	38.62 [104]	27.2	29 – 31	21.1	$18 \pm 1.5$ [6], 30, 32 [12]
MoSe <sub>2</sub>	0.38	0.44	51.71 [33]	25.3	29 – 31	21.3	30 [7, 10]
WS <sub>2</sub>	0.27	0.32	37.89 [33]	29.1	28 – 30	22.5	30 [16], 45 [13]
WSe <sub>2</sub>	0.29	0.34	45.11 [33]	27.5	28 – 30	21.8	30 [8, 9]

The examination of the results in Table I reveals that in the short-range limit,  $r \ll \rho_0$ , the binding energies are less than experimental values for MoSe<sub>2</sub>, WS<sub>2</sub> and WSe<sub>2</sub>. The binding energy of  $X^-$  in MoSe<sub>2</sub> monolayer is also less than experimental data reported in Ref. [12]. The same behaviors are observed for the long-range limit,  $r \gg \rho_0$ . However, results with the logarithmic potential are always larger than those with the Coulomb potential. It is worth noting that the binding energies obtained for the short-range limit are in reasonable agreement with calculations [39], in which trions were treated as three logarithmically interacting particles. Thus, analytical expressions (26) and (36) provide reasonable estimates for trion binding energies in TMDC monolayers.

### C. Binding energies of $X^-$ and $X^+$ trions

While we can obtain the analytical expressions for the trion binding energy and wave functions in both the long- and short-range limits within the diagonal approximation, it is impossible to solve the trion problem analytically when charged carriers interact via the centrally symmetric RK potential. This conclusion follows based on the Nikiforov-Uvarov approach [106]: if there exists a class of transformations which allows us to transform the three-body radial Schrödinger equation with potential (2) into an equation of the simpler form  $F(r)\frac{d^2u(r)}{dr^2} + f(r)\frac{du(r)}{dr} + \xi u(r) = 0$ , where  $F(r)$  and  $f(r)$  are polynomials of at most the second and the first degree, respectively, and  $\xi$  is a constant, the corresponding equation can be solved analytically within the theory of special functions. To the best of our knowledge no one has found, at least by today, such a transformation for the three-body radial Schrödinger equation with RK potential (2). Noticing that the modified Kratzer potential considered in Ref. [107] for excitons description can be used to calculate the binding energy of trions. For the modified Kratzer potential, follow [87] and using the approach presented for the long-range limit, one can obtain in the diagonal approximation the analytical expression for the binding energy and wave function for trions in terms of the Laguerre polynomials.

TABLE II: Convergence of binding energies for the freestanding bright  $X^-$  trion in meV. The electron and hole effective masses are taken from Ref. [1].

TMDC	$K = 0$	$K = 0, 2$	$K = 0, 2, 4$	$K = 0, 2, 4, 6$	$K = 0, 2, 4, 6, 8$	$K = 0, 2, 4, 6, 8, 10$
Binding Energy, meV						
MoS <sub>2</sub>	28.8	29.9	31.9	32.6	32.78	32.80
MoSe <sub>2</sub>	24.5	26.6	26.9	27.4	27.6	27.6
WS <sub>2</sub>	30.1	32.3	32.6	32.8	33.0	33.1
WSe <sub>2</sub>	24.5	25.5	27.2	27.8	28.2	28.3

The system of coupled differential equations (13) for the hyperradial functions  $u_{K\lambda}^L(\rho)$  are solved numerically. By solving the system of equations (13) one finds the binding energy as well as the corresponding hyperradial functions. The latter allows one to construct the wave function (12). The convergence of the binding energies for trions with respect to the grand angular momentum  $K$  is given in Table II. The relative convergence is checked as  $\Delta B/B = [B(K+2) - B(K)]/B(K)$ , where  $B(K)$  is the binding energy for the given  $K$ . The analysis of the results in Table II shows that the reasonable convergence is reached for  $K_{\max} = 12$ , so we limit our considerations to this value. The dependence of hyperradial wave functions on hyperradius  $\rho$  for a trion obtained in the short-range limit (logarithmic potential) long-range limit (the Coulomb potential), and for the Rytova-Keldysh potential are shown in Fig. 4.

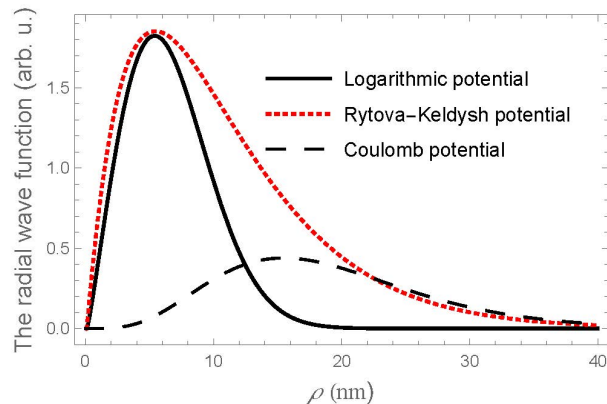


FIG. 4: (Color online) Dependence of the hyperradial wave function on hyperradius  $\rho$  for the logarithmic, Coulomb, and Rytova-Keldysh potentials.

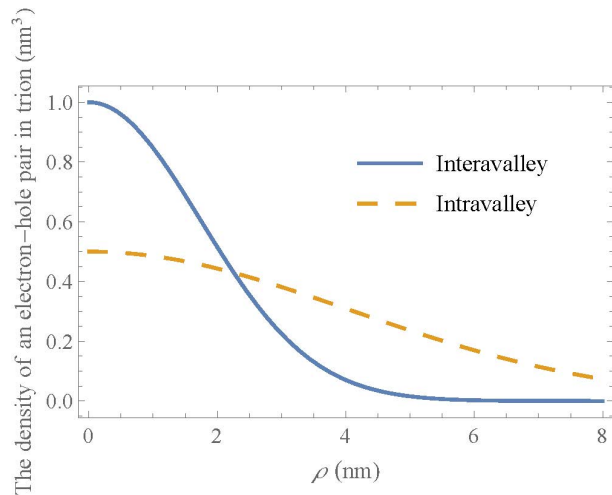


FIG. 5: (Color online) Probability density distribution for the intervalley and intravalley electron-hole pair.

The results of our calculations for the binding energies of the trions in freestanding, supported by dielectric  $\text{SiO}_2$ , and encapsulated by hBN  $\text{MoS}_2$ ,  $\text{MoSe}_2$ ,  $\text{WS}_2$ , and  $\text{WSe}_2$  monolayers, are presented in Table III. The dielectric environment of an atomically-thin monolayer of TMDC affects both the electronic band gap and the excitonic binding energy in the monolayer. In our calculations, the role of the substrate and the encapsulation by hBN is considered through the potential (2) with  $\epsilon = (\epsilon_1 + \epsilon_2)/2$ , where  $\epsilon_1$  and  $\epsilon_2$  are the dielectric constants of two materials that the TMDC layer is surrounded by. More quantitative treatments of substrate and heterostructure screening effects can be achieved with the quantum electrostatic heterostructure approach developed in Refs. [108, 109]. In addition to the intrinsic dielectric response of a monolayer TMDC and its electronic environment, a number of other potential sources of screening should be considered for a fully quantitative theory [49, 108]. However, even in our simple approach one finds a strong dependence of the binding energy on whether the TMDC monolayer is freestanding in air, supported on  $\text{SiO}_2$ , or encapsulated in the hexagonal boron-nitride.

The masses of electrons and holes in TMDC materials are of similar but not the same magnitude. Following *ab*

TABLE III:  $X^-$  and  $X^+$  bright trions binding energies in meV in the freestanding,  $\text{SiO}_2$  - supported, and hBN - encapsulated TMDC monolayers. The electron and hole effective masses are taken from Ref. [1]. Effective masses of electrons from  $K$  and  $K'$  valleys are the same.  $m_0$  is the free electron mass.

	Input parameters			Suspended		Supported	Encapsulated
	$m_e/m_0$	$m_h/m_0$	$\rho_0, \text{\AA}$	$X^-$	$X^+$	$X^-$	$X^-$
MoS <sub>2</sub>	0.350	0.428	38.62 [104]	32.80	33.2	25.1	23.3
MoSe <sub>2</sub>	0.38	0.44	51.71 [33]	27.6	28.8	20.2	18.4
WS <sub>2</sub>	0.27	0.32	37.89 [33]	33.1	33.2	25.6	22.4
WSe <sub>2</sub>	0.29	0.34	45.11 [33]	28.6	28.9	21.4	18.2

TABLE IV: The binding energy of intervalley  $X^-$  and  $X^+$  freestanding, supported by  $\text{SiO}_2$  dielectric and encapsulated by hBN in the monolayer WSe<sub>2</sub>.

Binding energy of $X^-$ and $X^+$ trions in WSe <sub>2</sub> , meV			
	Freestanding	Supported	Encapsulated
Intravalley, singlet state, $L = 0, S = 1/2$			
$X^-, K$ valley electrons	28.6	21.4	18.2
$X^-, K'$ valley electrons	38.7	34.6	29.4
Intervalley, singlet state, $L = 0, S = 1/2$			
$X^+, K$ valley electron	28.9	22.9	19.8
$X^+, K'$ valley electron	29.4	24.5	21.6
Intervalley, triplet state, $L = 1, S = 3/2$			
$X^-, K, K'$ valley electrons	26.3	20.1	18.7

*initio* calculations [1], the effective masses of electrons and holes are different in the  $K$  and  $K'$  valleys. The effect of the different electron masses in the  $K$  and  $K'$  valleys on the binding energy of the trion was studied in Ref. [110]. At this point, intervalley  $X^-$  in tungsten-based compounds is unique because its electrons have different masses: one electron comes from the top spin-split of the conduction band of one valley, while the second electron comes from the other valley [21, 111, 112]. The difference of electron masses breaks the symmetry of the wave function and leads to the change in the binding energy due to the following: the  $X^-$  wave function is not antisymmetric with respect to the permutation of two electrons; the binding energy increases or decreases depending on the added excess electron mass. These differences are consequential since the binding energy of the trion is enhanced/suppressed when the added charge is heavier/lighter than the one with the same charge in the neutral exciton (recall that the trion binding energy is measured with respect to that of the exciton) [110]. As an example, we consider WSe<sub>2</sub> monolayer with the effective electron mass  $m_e = 0.29/m_0$  in one and  $m_e = 0.4/m_0$  in the other valley, while the hole mass in the top valence band  $m_h = 0.34/m_0$  is less than the mass of the added excess electron mass. The effect of different electron masses from  $K$  and  $K'$  valleys on the probability density distribution for the intervalley and intravalley electron-hole pair is demonstrated in Fig. 5. We calculate a probability distribution for three particles that form a trion. In Fig. 6a interparticle radial probability distributions for intravalley and intervalley  $X^-$  trions are shown. The difference in the probability distribution is related to the difference of the effective masses of electrons in  $K$  and  $K'$  and the symmetry of trion wave function in different valleys: the singlet state  $X^-$  trion (Fig. 6a, solid curve) wave function is antisymmetric with respect to the permutation of two electrons in the  $K$  valley, while for the singlet state  $X^-$  intervalley trion (Fig. 6a, dotted curve) with different effective electron masses in the  $K$  and  $K'$  valleys, the symmetry of the wave function is broken. In Figs. 6b and 6c the dependence of the probability distribution of three particles on the hyperradius  $\rho$  and the electron and hole masses ratio is shown. With the increase of the ratio  $m_e/m_h$ , the particles become more compact localized and, hence, more strongly bound.

We calculate the binding energies of trions when electrons in  $K$  and  $K'$  valleys have different effective masses. Let us consider dark  $X^-$  and  $X^+$  trions in the spin-valley configuration shown in Figs. 3e and 3h, respectively. In Ref. [23] observed both the positive and negative dark trions in WSe<sub>2</sub> under continuous electrostatic gating. The dark trions can be tuned continuously between  $X^-$  and  $X^+$  trions with electrostatic gating [23]. The bright trions have a higher energy in the range of 21–35 meV. Compared to bright trions, dark trions in WSe<sub>2</sub> have smaller, but still sizable, binding energies 14–16 meV [23]. The authors reveal the spin-triplet configuration and distinct valley

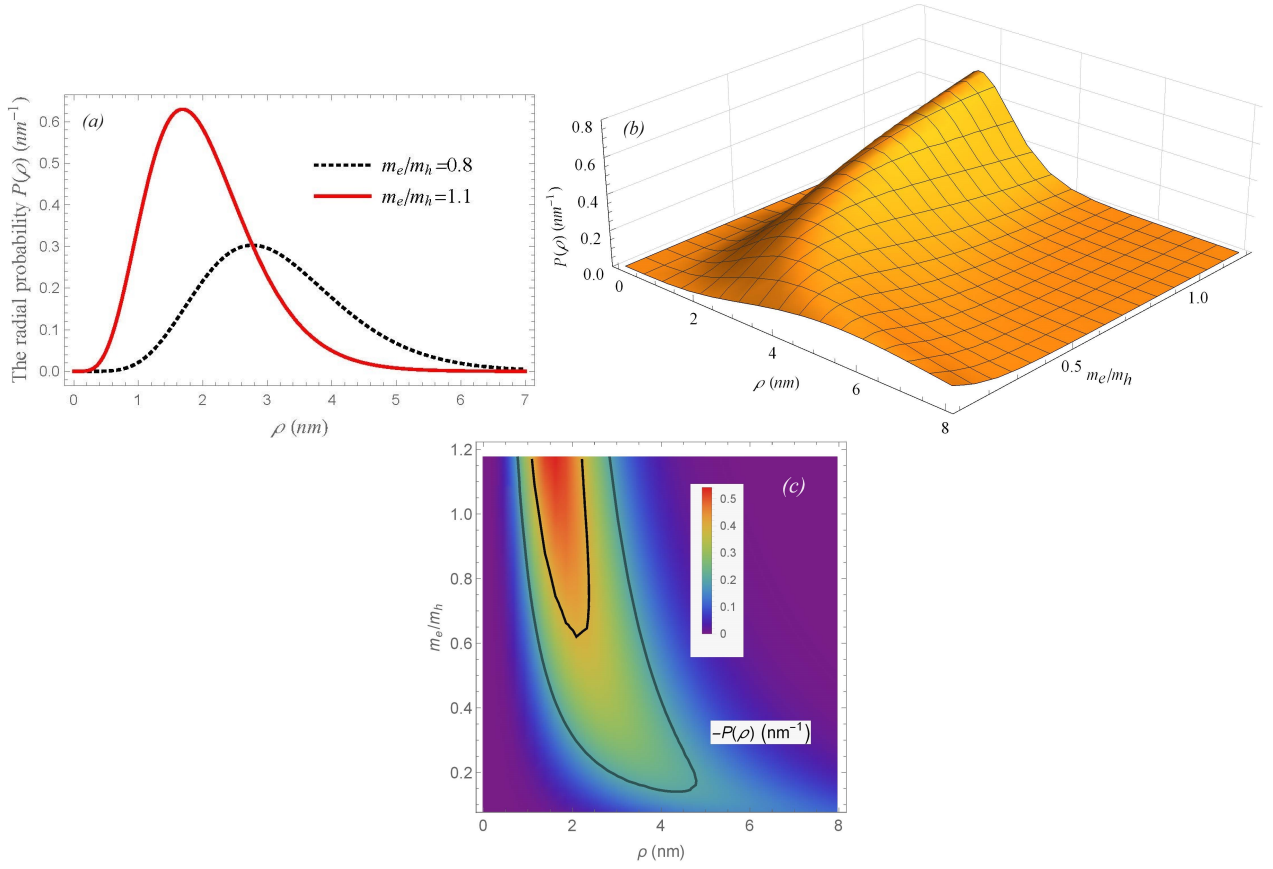


FIG. 6: (Color online) (a) Radial probability distribution for fixed  $m_e/m_h$  ratio. (b, c) Dependence of the probability distribution of three particles on hyperradius  $\rho$  and  $m_e/m_h$  ratio.

optical emission of dark trions by their characteristic Zeeman splitting under a magnetic field. Our calculations for the boron nitride-encapsulated  $X^-$  spin-triplet configuration (Fig. 3e) reveals the binding energy 15.6 meV. For the dark spin-singlet  $X^+$  (Fig. 3h) we obtained 14.2 meV. These results match the theoretical prediction (15 meV) [43] and the reported experimental value.

The analysis of binding energies will help us to understand the energy difference between the binding energies of positive and negative trions in molybdenum-based and tungsten-based TMDCs. As we mentioned above, in the case when electrons are from different valleys, the wave function of the intravalley  $X^-$  trion has no symmetry and should not be antisymmetric with respect to the permutation of two electrons. Results of calculations for the binding energy of freestanding,  $\text{SiO}_2$ -supported, and hBN-encapsulated monolayer  $\text{WSe}_2$  intervalley  $X^-$  and  $X^+$  are presented in Table IV. For a comparison, the same Table presents binding energies for the intravalley  $X^-$  and intervalley  $X^+$  trions formed with electrons from the  $K$  and  $K'$  valleys, respectively. The analysis of the results leads to the following conclusions: i. the binding energies of  $X^-$  and  $X^+$  trions with electrons from the  $K$  valley are always smaller; ii. the binding energy of the  $X^-$  trion in the state  $L = 1$  and  $S = 3/2$  with electrons from the  $K$  and  $K'$  valleys is the smallest; iii. the screening substantially decreases the binding energies of both the  $X^-$  and  $X^+$  trions. To understand these patterns, for simplicity, consider the analytical expression for the ground state energy (26) in the diagonal approximation, which allows us to obtain a physically transparent picture of the dependence of the trion binding energy on the effective masses of constituent quasiparticles. One can see the explicit dependence of the energy on the three-particle effective mass  $\mu$  given by Eq. (26). The increase of  $\mu$  leads to the increase of the binding energy of the trion. The larger binding energies of  $X^-$  and  $X^+$  trions formed with electrons from the  $K'$  valley is due to the larger their three-particle effective mass. The decrease of the  $X^-$  binding energy in the state  $L = 1$  and  $S = 3/2$  is due to the centrifugal repulsion and different three-particle effective mass obtained with the masses of  $K$  and  $K'$  valley electrons.

Results of our calculations show the strong correlation between binding energies of  $X^-$  and  $X^+$  trions and the constituent masses: more massive holes correspond to larger binding energies of  $X^+$  trions. The binding energy of intervalley  $X^-$  is larger than that of  $X^+$  trions if the mass of one of the valley electrons  $m_e > m_h$ .

## V. CONCLUSIONS

We develop the theoretical formalism and study the formation of valley trions in two-dimensional materials within the framework of a non-relativistic potential model using the method of hyperspherical harmonics in four-dimensional space. We solve the three-body Schrödinger equation with the Rytova-Keldysh potential by expanding the wave functions of a trion in terms of the HH. The antisymmetrization of the wave functions of  $X^-$  and  $X^+$  trions is based on the electron and hole spins and valley indices, in case of two identical electrons or two identical holes. In the case of  $X^-$ , when the two intravalley electrons could have unequal masses, calculations are performed by solving the Schrödinger equation for three indistinguishable particles. We applied our theoretical approach to trions in TMDC and demonstrated that the proposed theory is capable of describing trions in TMDCs

We considered the long-range approximation when the RK potential can be approximated by the Coulomb potential and the short-range limit when this potential is approximated by the logarithmic potential. In the diagonal approximation in both limits, the system of differential equations for the hyperradial functions is decoupled. Our approach yields the analytical solution for binding energies of trions in the diagonal approximation for these two limiting cases - the Coulomb and logarithmic potentials. We obtained the exact analytical expressions for eigenvalues and eigenfunctions for  $X^-$  and  $X^+$  trions. The corresponding energies can be considered as the lower and upper limits for the trion binding energies.

The system of coupled differential equations for the hyperradial functions  $u_{K\lambda}^L(\rho)$  can be solved efficiently with fairly accurate results. In our approach, results for the binding energies depend on input parameters and spin-valley symmetry description of  $X^-$  and  $X^+$  trions. On one hand, the difference in binding energy between  $X^+$  and  $X^-$  is related to the effective masses of the electrons and hole as well as screening distance for TMDC monolayers. On the other hand, spin-valley quantum numbers combination. The latter leads to the existence of bright and dark trions. The binding energies of dark trions are less than binding energies of the bright trions.

Let us note that different methods of calculations of the electron and hole masses give slightly different effective masses. Thus, in our approach, where the effective electron and hole masses are input parameters, we show that trion binding energies are sensitive to these parameters and depend on the wave function symmetry. Results of our calculations show the strong correlation between binding energies of  $X^-$  and  $X^+$  trions and the electron and hole masses. The more massive holes correspond to larger binding energies of  $X^+$  trions. When the mass of one of electrons form one valley  $m_e > m_h$ , the binding energy of intervalley  $X^-$  is larger than that of  $X^+$ . Results of numerical calculations for the ground state energies are in good agreement with similar calculations for the Rytova-Keldysh potential and in fair agreement with the reported experimental measurements for trion binding energies.

As mentioned in the introduction, there have been many other methods to calculate the trion binding energy. All these methods are quite powerful to study trions and give close results for binding energies, which are in reasonable agreement with experimental measurements. The HH formalism yields the analytical solution for binding energy and wave function of trions in the diagonal approximation for the Coulomb and logarithmic potentials, allows direct access to the wave functions, and explicit analysis of the dependence of  $X^-$  and  $X^+$  binding energies on the effective masses of constituent particles.

### Appendix A: Evaluation of the $\mathcal{G}_{K\lambda K'\lambda'}^L$ for the Coulomb potential

For the Coulomb potential the  $\mathcal{G}_{K\lambda K'\lambda'}^L$  can be evaluated analytically. Let us write (23) using the corresponding set of  $\Omega_i \equiv (\alpha_i, \hat{\mathbf{x}}_i, \hat{\mathbf{y}}_i)$  angles

$$\begin{aligned} \mathcal{G}_{K\lambda K'\lambda'}^L = ke^2 \left\{ b_1 \int \Phi_{K\lambda}^{L*}(\Omega_i) \left( \frac{1}{\cos \alpha_1} \right) \Phi_{K'\lambda'}^{L'}(\Omega_1) d\Omega_1 - \right. \\ \left. b_2 \sum_{\lambda_k \lambda'_k} \langle \lambda_k | \lambda_i \rangle_{KL} \langle \lambda'_k | \lambda_i \rangle_{KL} \int \Phi_{K\lambda}^{L*}(\Omega_2) \left( \frac{1}{\cos \alpha_2} \right) \Phi_{K'\lambda'}^{L'}(\Omega_2) d\Omega_2 - \right. \\ \left. b_3 \sum_{\lambda_j \lambda'_j} \langle \lambda_j | \lambda_i \rangle_{KL} \langle \lambda'_j | \lambda_i \rangle_{KL} \int \Phi_{K\lambda}^{L*}(\Omega_3) \left( \frac{1}{\cos \alpha_3} \right) \Phi_{K'\lambda'}^{L'}(\Omega_3) d\Omega_3 \right\} \quad (\text{A1}) \end{aligned}$$

The values of all integrals in (A1) are the same and for the integral (24) we finally obtain



$$\begin{aligned}
\mathcal{C}_{K\lambda K'\lambda'}^{(i)} &= \int \Phi_{K\lambda}^{L*}(\Omega) \left( \frac{1}{\cos \alpha} \right) \Phi_{K'\lambda'}^{L'}(\Omega) d\Omega = \int \Phi_{K\lambda}^{L*}(\Omega) \left( \frac{1}{\cos \alpha} \right) \Phi_{K'\lambda'}^{L'}(\Omega) \cos \alpha \sin \alpha d\alpha d\varphi_x d\varphi_y = \\
&\frac{1}{2} N_K^{\{l\}} N_{K'}^{\{l'\}} \delta_{l_1 l_2} \delta_{l'_1 l'_2} \delta_{LL'} \delta_{MM'} \Gamma(n + l_1 + 1/2) \Gamma(n + l_2 + 1/2) \times \\
&\Gamma(n' + l_1 + 1/2) \Gamma(n' + l_2 + 1/2) \times \\
&\sum_{\sigma=0}^n \sum_{\sigma'=0}^{n'} \left\{ \frac{(-1)^{n-\delta}}{\Gamma(\sigma + 1/2) \Gamma(\sigma + l_1 + 1/2) \Gamma(n - \sigma + l_2 + 1/2) \Gamma(n - \sigma + 1)} \times \right. \\
&\left. \frac{(-1)^{n'-\delta'}}{\Gamma(\sigma' + 1/2) \Gamma(\sigma' + l_1 + 1/2) \Gamma(n' - \sigma' + l_2 + 1/2) \Gamma(n' - \sigma' + 1)} \times \right. \\
&\left. B[l_1 + \sigma + \sigma' + 1, l_2 + (n + n') - (\sigma + \sigma') + 1/2] \right\}, \tag{A2}
\end{aligned}$$

with  $\Gamma$  and  $B$  indicating the standard Gamma and Beta functions [73, 74], respectively,  $n = (K - l_1 - l_2)/2$ , and  $n' = (K' - l'_1 - l'_2)/2$ .

### Appendix B: Evaluation of the $\mathcal{L}_{K\lambda K'\lambda'}^{(i)}$ for the logarithmic potential

Let us consider the evaluation of  $\mathcal{L}_{K\lambda K'\lambda'}^{(i)}$  defined in Eq. (32)

$$\begin{aligned}
\mathcal{L}_{K\lambda K'\lambda'}^{(i)} &= \int \Phi_{K\lambda}^{L*}(\Omega_i) \ln \cos \alpha \Phi_{K'\lambda'}^{L'}(\Omega) d\Omega = \int \Phi_{K\lambda}^{L*}(\Omega) \ln \cos \alpha \Phi_{K'\lambda'}^{L'}(\Omega) \cos \alpha \sin \alpha d\alpha d\varphi_x d\varphi_y = \\
&\frac{1}{4} N_K^{\{l\}} N_{K'}^{\{l'\}} \delta_{l_1 l_2} \delta_{l'_1 l'_2} \delta_{LL'} \delta_{MM'} \sum_{\sigma=0}^n \sum_{\sigma'=0}^{n'} \left\{ \binom{\sigma + l_1}{\sigma} \binom{\sigma + l_2}{n - \sigma} \binom{\sigma' + l'_1}{\sigma'} \binom{\sigma + l'_2}{n' - \sigma'} \times \right. \\
&H[1/2\sigma l_1 + l'_1 + \sigma'] - H[1/2(3 - 2\sigma + 2n + \sigma l_1 + l_2 + l'_1 - 2(-1 + l'_2 \sigma' + 2l'_2 n')] \times \\
&\left. \frac{\Gamma(\sigma + \sigma l_1 + 1/2 l'_1 + \sigma') \Gamma(3/2 - \sigma + n + 1/2 l_2 + l'_2 (n' - \sigma'))}{\Gamma(2\sigma' + n + 1/2 l_2 + \sigma l_1 + 1/2 l'_1 + l'_2 (\sigma - n') + 3/2)} \right\}, \tag{B1}
\end{aligned}$$

where  $H[z]$  is a Harmonic number.

### Appendix C: Reduction of Eq. (34) to the Weber's equation

The logarithmic potential is widely used as a quark confinement potential in high energy physics with applications to elementary particle spectroscopy. There is no known complete analytical solution of the Schrödinger equation for a logarithmic potential. However, there is known an almost complete solution of the Schrödinger equation for a logarithmic potential [88–90]. Following the methodology [89] by the rescaling of variable  $\rho$  and introducing a new function, one can reduce (34) to the equation for the parabolic cylinder function known Weber's equation [91]. Let us rescale variable  $\rho$  by introducing the new variable  $z$  as

$$\rho = e^{z - \alpha/\beta}, \quad (-\infty < z < \infty) \tag{C1}$$

and set the solution of Eq. (34) in the form

$$u_{K\lambda} = e^{z - \alpha/\beta} \Phi(z). \tag{C2}$$

Using (C1) and (C2) one can rewrite (34) in the following form

$$\frac{d^2 \Phi(z)}{dZ^2} + [-\Delta^2 + V(z)] \Phi(z) = 0, \tag{C3}$$

where  $\Delta^2 = (K + 1)^2$  and

$$V(z) = -z\beta e^{2\alpha/\beta + 2z}. \tag{C4}$$

The function  $V(z)$  is twice differentiable at a stationary point  $z_0$ . Finding the existence of eigenvalues for differential equations is a boundary value problem:  $-\Delta^2 + V(z)$  must be positive and in the vicinity of the maximum value of  $V(z)$ , where  $-\Delta^2 + V(z) > 0$  Eq. (C3) leads to an oscillatory type solution. Let us find the value of  $z = z_0$  for which  $V(z)$  has a maximum. In the vicinity of this maximum  $-\Delta^2 + V(z)$  can become positive. The condition for the derivative  $\frac{dV(z)}{dz} = 0$  and  $\left. \frac{d^2V(z)}{dz^2} \right|_{z=z_0} < 0$  yields the value  $z_0 = -\frac{1}{2}$ . Expanding  $V(z)$  in a Taylor series in the neighborhood of the maximum at  $z_0$ , we obtain in the first order with respect to  $(z - z_0)^2$

$$V(z) = V(z_0) + \frac{z - z_0}{2!} V''(z_0) + \dots, \quad (\text{C5})$$

where

$$V''(z_0) = -4\beta e^{2\alpha/\beta + 2z_0} (1 + z_0). \quad (\text{C6})$$

Let's set the new variable

$$w = S(z - z_0), \quad \text{where } S = \sqrt[4]{4\beta e^{(2\alpha - \beta)/\beta}}. \quad (\text{C7})$$

Applying (C7) to (C3), we have

$$\left[ \frac{d^2\Phi(z)}{dw^2} + \frac{-\Delta^2 + 1/8S^4}{S^2} - \frac{1}{4}w^2 \right] \Phi(w) = \sum_{i=3}^{\infty} \frac{(i-1)2^{i-3}}{i!} \frac{w^i}{s^{i-2}} \Phi(w). \quad (\text{C8})$$

Neglecting the right side in the latter equation, we obtain

$$\left[ \frac{d^2\Phi(z)}{dw^2} + \frac{-\Delta^2 + 1/8S^4}{S^2} - \frac{1}{4}w^2 \right] \Phi(w) = 0. \quad (\text{C9})$$

The eigenvalues and eigenfunctions for the a boundary value problem for Eq. (C9) with the vanishing wave function at infinity can be obtained by comparing this equation with the equation for the parabolic cylinder functions. This comparison requires that the solution of (C9) be square-integrable only if

$$\frac{-\Delta^2 + 1/8S^4}{S^2} = \frac{(2n+1)}{2}, \quad n = 0, 1, 2, \dots \quad (\text{C10})$$

Equation (C10) can be reduced to the following biquadratic equation

$$S^4 - 4(2n+1)S^2 - 8\Delta^2 = 0, \quad n = 0, 1, 2, \dots \quad (\text{C11})$$

with solution

$$S^2 = 2(2n+1) + 2[(2n+1)^2 + 2\Delta^2]^{1/2}. \quad (\text{C12})$$

After substituting (C7) into Eq. (C12), we get

$$2\beta e^{(2\alpha - \beta)/2\beta} = 4 \left( (2n+1) + [(2n+1)^2 + 2\Delta^2]^{1/2} \right)^2. \quad (\text{C13})$$

Therefore,

$$\beta e^{(2\alpha - \beta)/2\beta} = 2 \left( (2n+1) + [(2n+1)^2 + 2\Delta^2]^{1/2} \right)^2, \quad (\text{C14})$$

$$\ln\beta + \ln e^{(2\alpha - \beta)/2\beta} = 2\ln 2 \left( (2n+1) + [(2n+1)^2 + 2\Delta^2]^{1/2} \right) \quad (\text{C15})$$

or finally

$$\alpha = \ln 2 \left( (2n+1) + [(2n+1)^2 + 2\Delta^2]^{1/2} \right) - \frac{\ln\beta + \beta}{2}. \quad (\text{C16})$$

Thus,

$$\kappa^2 = \ln 2 \left( (2n+1) + [(2n+1)^2 + 2\Delta^2]^{1/2} \right) - \frac{\ln \beta + \beta}{2} + \frac{2\mu}{\hbar^2} \left( -\frac{ke^2}{\epsilon\rho_0} \ln \rho_0 + \mathcal{B}_{123} + \mathcal{J}_{K\lambda K\lambda} \right). \quad (\text{C17})$$

The eigenfunctions that correspond to these eigenvalues are

$$\Phi = D_n(w) = 2^{(n-1)/2} e^{-w^2/4} F\left(\frac{1-n}{2}, \frac{3}{2}, \frac{w^2}{2}\right), \quad (\text{C18})$$

where  $w$  is defined by Eq. (C7) and  $F(\frac{1-n}{2}, \frac{3}{2}, \frac{w^2}{2})$  is a confluent hypergeometric function.

- 
- [1] A. Kormányos, G. Burkard, M. Gmitra, et al.,  $k \cdot p$  theory for two-dimensional transition metal dichalcogenide semiconductors. *2D Mater.* **2**, 022001 (2015).
- [2] M. A. Lampert, Mobile and immobile effective-mass-particle complexes in nonmetallic solids. *Phys. Rev. Lett.* **1**, 450 (1958).
- [3] K. Kheng, R. T. Cox, M. Y. d' Aubigné, F. Bassani, et al., Observation of negatively charged excitons  $X^-$  in semiconductor quantum wells. *Phys. Rev. Lett.* **71**, 1752 (1993).
- [4] G. Finkelstein, H. Shtrikman, I. Bar-Joseph, Shakeup processes in the recombination spectra of negatively charged excitons. *Phys. Rev. B* **53** R1709 (1996)
- [5] I. Filikhin, R. Ya. Kezerashvili, Sh. M. Tsiklauri, and B. Vlahovic, Trions in bulk and monolayer materials: Faddeev equations and hyperspherical harmonics. *Nanotechnology* **29**, 124002 (2018).
- [6] K. F. Mak, K. He, C. Lee, et al., Tightly bound trion in monolayer  $\text{MoS}_2$ . *Nat. Mater.* **12**, 207 (2013).
- [7] J. S. Ross, S. Wu, H. Yu, et al., Electrical control of neutral and charged excitons in a monolayer semiconductor. *Nat. Comm.* **4**, 1474 (2013).
- [8] A. M. Jones, H. Yu, N. J. Ghimire, et al., Optical generation of excitonic valley coherence in monolayer  $\text{WSe}_2$ . *Nat. Nanotechnol.* **8**, 634 (2013).
- [9] G. Wang, L. Bouet, D. Lagarde, et al., Valley dynamics probed through charged and neutral exciton emission in monolayer  $\text{WSe}_2$ . *Phys. Rev. B* **90**, 075413 (2014).
- [10] A. Singh, G. Moody, S. Wu, et al., Coherent electronic coupling in atomically thin  $\text{MoSe}_2$ . *Phys. Rev. Lett.* **112**, 21680 (2014).
- [11] C. H. Lui, A. J. Frenzel, D. V. Pilon, et al., Trion-induced negative photoconductivity in monolayer  $\text{MoS}_2$ . *Phys. Rev. Lett.* **113**, 166801 (2014).
- [12] C. Zhang, H. Wang, W. Chan, C. Manolatou, and R. Rana, Absorption of light by excitons and trions in monolayers of metal dichalcogenide  $\text{MoS}_2$ : Experiments and theory *Phys. Rev. B* **89**, 205436 (2014).
- [13] B. Zhu, H. Zeng, J. Dai, Z. Gong, and X. Cui, Anomalous robust valley polarization and valley coherence in bilayer  $\text{WS}_2$ . *Proc. Natl. Acad. Sci. U.S.A.* **111**, 11606 (2014).
- [14] J. Yang, T. Lü, Y. W. Myint, J. Pei, D. Macdonald, J. Zheng, and Y. Lu, Robust excitons and trions in monolayer  $\text{MoTe}_2$ . *ACS Nano* **9**, 6603 (2015).
- [15] J. Shang, X. Shen, C. Cong, N. Peimyoo, B. Cao, M. Eginligil, and T. Yu, Observation of excitonic fine structure in a 2D transition-metal dichalcogenide semiconductor. *ACS Nano* **9**, 647 (2015).
- [16] G. Plechinger, P. Nagler, J. Kraus, N. Paradiso, C. Strunk, C. Schüller, and T. Korn, Identification of excitons, trions and biexcitons in single-layer  $\text{WS}_2$ . *Phys. Status Solidi RRL* **9**, 457 (2015).
- [17] Y. Zhang, H. Li, H. Wang, R. Liu, S. Zhang, and Z. Qiu, On valence-band splitting in layered  $\text{MoS}_2$ . *ACS Nano* **9**, 8514 (2015).
- [18] A. Singh, G. Moody, K. Tran, et al., Trion formation dynamics in monolayer transition metal dichalcogenides, *Phys. Rev. B* **93**, 041401(R) (2016).
- [19] M. Drüppel, T. Deilmann, P. Krüger, and M. Rohlfing, Diversity of trion states and substrate effects in the optical properties of an  $\text{MoS}_2$  monolayer. *Nat. Commun.* **8**(1), 2117 (2017).
- [20] J. W. Christopher, B. B. Goldberg, and A. K. Swan, Long-tailed trions in monolayer  $\text{MoS}_2$ : temperature dependent asymmetry and resulting red-shift of trion photoluminescence spectra. *Sci. Rep.* **7**, 14062 (2017).
- [21] E. Courtade, M. Semina, M. Manca, et al., Charged excitons in monolayer  $\text{WSe}_2$ : experiment and theory. *Phys. Rev. B* **96**, 085302 (2017).
- [22] F. Volmer, S. Pissinger, M. Ersfeld, S. Kuhlen, C. Stampfer, and B. Beschoten, Intervalley dark trion states with spin lifetimes of 150 ns in  $\text{WSe}_2$ . *Phys. Rev. B* **95**, 235408 (2017).
- [23] E. Liu, J. van Baren, Z. Lu, et al., Gate tunable dark trions in monolayer  $\text{WSe}_2$ . *Phys. Rev. Lett.* **123**, 027401 (2019).
- [24] S. Borghardt and B. E. Kardynal, Interplay of excitonic complexes in p-doped  $\text{WSe}_2$  monolayers. *Phys. Rev. B* **101**, 161402(R) (2020).
- [25] M. Zinkiewicz, M. Grzeszczyk, L. Kipczak, et al., The effect of dielectric environment on the brightening of neutral and charged dark excitons in  $\text{WSe}_2$  monolayer. *Appl. Phys. Lett.* **120**, 163101 (2022).

- [26] J. Klein, M. Florian, A. Hotger, et al., Trions in MoS<sub>2</sub> of intra- and intervalley spin states. *Phys. Rev. B* **105**, L041302 (2022).
- [27] K-Q. Lin, et al., High-lying valley-polarized trions in 2D semiconductors. *Nat. Comm.* **13**, 6980 (2022).
- [28] H. Yu, X. Cui, X. Xu, and W. Yao, Valley excitons in two-dimensional semiconductors. *Natl. Science Rev.* **2**, 57 (2015).
- [29] T. C. Berkelbach and D. R. Reichman, Optical and excitonic properties of atomically thin transition-metal dichalcogenides, *Annu. Rev. Condens. Matter Phys.* 2018. **9**, 379–96 (2018).
- [30] M. V. Durnev and M. M. Glazov, Excitons and trions in two-dimensional semiconductors based on transition metal dichalcogenides, *Phys.-Usp.* **61**, 825 (2018).
- [31] R. Ya. Kezerashvili, Few-Body Systems in Condensed Matter Physics. *Few-Body Syst.* **60**, 52 (2019).
- [32] M. A. Semina and R. A. Suris, Localized excitons and trions in semiconductor nanosystems. *Phys.-Usp.* **65**, 111 (2022).
- [33] T. C. Berkelbach, M. S. Hybertsen, and D. R. Reichman, Theory of neutral and charged excitons in monolayer transition metal dichalcogenides. *Phys. Rev. B* **88**, 045318 (2013).
- [34] A. Ramirez-Torres, V. Turkowski, and T. S. Rahman, Time-dependent density-matrix functional theory for trion excitations: Application to monolayer MoS<sub>2</sub> and other transition-metal dichalcogenides. *Phys. Rev. B* **90**, 085419 (2014).
- [35] M. Z. Mayers, T. C. Berkelbach, M. S. Hybertsen, and D. R. Reichman, Binding energies and spatial structures of small carrier complexes in monolayer transition-metal dichalcogenides via diffusion Monte Carlo. *Phys. Rev. B* **92**, 161404 (2015).
- [36] Kylänpää I. and H.-P. Komsa, H.-P.: Binding energies of exciton complexes in transition metal dichalcogenide monolayers and effect of dielectric environment. *Phys. Rev. B* **92**, 205418 (2015).
- [37] K. A. Velizhanin and A. Saxena, Excitonic effects in 2D semiconductors: path integral Monte Carlo approach. *Phys. Rev. B* **92**, 195305 (2015).
- [38] D. K. Zhang, D. W. Kidd, and K. Varga, Excited biexcitons in transition metal dichalcogenides, *Nano Lett.* **15**, 7002 (2015).
- [39] B. Ganchev, N. Drummond, I. Aleiner, and V. Fal'ko, Three-particle complexes in two-dimensional semiconductors. *Phys. Rev. Lett.* **114**, 107401 (2015).
- [40] D. W. Kidd, D. K. Zhang, and K. Varga, Binding energies and structures of two-dimensional excitonic complexes in transition metal dichalcogenides. *Phys. Rev. B* **93**, 125423 (2016).
- [41] M. Szyniszewski, E. Mostaani, N. D. Drummond, and V. I. Fal'ko, Binding energies of trions and biexcitons in two-dimensional semiconductors from diffusion quantum Monte Carlo calculations. *Phys. Rev. B* **95**, 081301(R) (2017).
- [42] E. Mostaani, M. Szyniszewski, C. H. Price, R. Maezono, M. Danovich, et al., Diffusion quantum Monte Carlo study of excitonic complexes in two-dimensional transition-metal dichalcogenides. *Phys. Rev. B* **96**, 075431 (2017).
- [43] T. Deilmann and K. S. Thygesen, Dark excitations in monolayer transition metal dichalcogenides. *Phys. Rev. B* **96**, 201113(R) (2017).
- [44] M. Danovich, V. Zolyomi, and V. I. Fal'ko, Dark trions and biexcitons in WS<sub>2</sub> and WSe<sub>2</sub> made bright by e-e scattering. *Sci. Rep.* **7**, 45998 (2017).
- [45] R. Ya. Kezerashvili and Sh. M. Tsiklauri, Trion and biexciton in monolayer transition metal dichalcogenides. *Few-Body Syst.* **58**, 18 (2017).
- [46] D. K. Efimkin and A. H. MacDonald, Many-body theory of trion absorption features in two-dimensional semiconductors. *Phys. Rev. B* **95**, 035417 (2017).
- [47] M. Donck, M. Zarenia, and F. Peeters, Excitons, Trions, and Biexcitons in Transition-Metal Dichalcogenides: Magnetic-Field Dependence. *Physical Review B*, **97**, 195408 (2018).
- [48] L. S. R. Cavalcante, D. R. da Costa, G. A. Farias, D. R. Reichman, and A. Chaves, Stark shift of excitons and trions in two-dimensional materials, *Phys. Rev. B* **98**, 245309 (2018).
- [49] M. Florian, M. Hartmann, A. Steinhoff, et al., The dielectric impact of layer distances on exciton and trion binding energies in van der waals heterostructures. *Nano Lett.* **18**, 2725 (2018).
- [50] A. Torche and G. Bester, First-principles many-body theory for charged and neutral excitations: Trion fine structure splitting in transition metal dichalcogenides. *Phys. Rev. B* **100**, 201403(R) (2019).
- [51] D. V. Tuan, A. M. Jones, M. Yang, X. Xu, and H. Dery, Virtual trions in the photoluminescence of monolayer transition-metal dichalcogenides. *Phys. Rev. Lett.* **122**, 217401 (2019).
- [52] J. Fu, J. M. R. Cruz, and F. Qu, Valley dynamics of different trion species in monolayer WSe<sub>2</sub>. *Appl. Phys. Lett.* **115**, 082101 (2019).
- [53] J. Yan and K. Varga, Excited-state trions in two-dimensional materials. *Phys. Rev. B* **101**, 235435 (2020).
- [54] Y. V. Zhumagulov, A. Vagov, D. R. Gulevich, P. E. Faria Junior, and V. Perebeinos, Trion induced photoluminescence of a doped MoS<sub>2</sub> monolayer. *J. Chem. Phys.* **153**, 044132 (2020).
- [55] Y. V. Zhumagulov, A. Vagov, N. Yu. Senkevich, D. R. Gulevich, and V. Perebeinos, Three-particle states and brightening of intervalley excitons in a doped MoS<sub>2</sub> monolayer. *Phys. Rev. B* **101**, 245433 (2020).
- [56] M. Van der Donck, M. Zarenia, and F. M. Peeters, Excitons and trions in monolayer transition metal dichalcogenides: a comparative study between the multiband model and the quadratic single-band model. *Phys. Rev. B* **96**, 035131 (2017).
- [57] M. Glazov, Optical properties of charged excitons in two-dimensional semiconductors. *J. Chem. Phys.* **153**, 034703 (2020).
- [58] Y-W. Chang and Y-C. Chang, Variationally optimized orbital approach to trions in two-dimensional materials. *J. Chem. Phys.* **155**, 024110 (2021).
- [59] F. Marsusi, E. Mostaani, and N. D. Drummond, Quantum Monte Carlo study of three-dimensional Coulomb complexes: Trions and biexcitons, hydrogen molecules and ions, helium hydride cations, and positronic and muonic complexes. *Phys. Rev. A* **106**, 062822 (2022).

- [60] M. A. Semina, J. V. Mamedov, and M. M. Glazov, Excitons and trions with negative effective masses in two-dimensional semiconductors. *Oxford Open Materials Science*, **3**, itad004 (2023).
- [61] K. Mohseni, M. R. Hadizadeh, T. Frederico, D. R. da Costa, and A. J. Chaves, Trion clustering structure and binding energy in two-dimensional semiconductor materials: Faddeev equations approach. *Phys. Rev. B* **107**, 165427 (2023).
- [62] Y. Suzuki and K. Varga, *Stochastic Variational Approach to Quantum Mechanical Few-body Problems*, (Springer-Verlag, Berlin, 1998).
- [63] K. F. Mak, D. Xiao, and J. Shan, Light-valley interactions in 2D semiconductors. *Nat. Photon.* **12**, 451-460 (2018).
- [64] T. P. Lyons, S. Dufferwiel, M. Brooks, F. Withers, T. Taniguchi, K. Watanabe, et al., The valley Zeeman effect in inter- and intra-valley trions in monolayer WSe<sub>2</sub>. *Nat. Commun.* **10**, 2330 (2019).
- [65] Z. Li, T. Wang, Z. Lu, C. Jin, Y. Chen, Y. Meng, et al., Revealing the biexciton and trion-exciton complexes in BN encapsulated WSe<sub>2</sub>. *Nat. Commun.* **9**, 3719 (2018).
- [66] A. Arora, T. Deilmann, T. Reichenauer, J. Kern, et al., Excited-state trions in monolayer WS<sub>2</sub>. *Phys. Rev. Lett.* **123** 16, 167401 (2019).
- [67] J. Zipfel, K. Wagner, J. D. Ziegler, T. Taniguchi, K. Watanabe, M. A. Semina, and A. Chernikov, Light-matter coupling and non-equilibrium dynamics of exchange-split trions in monolayer WS<sub>2</sub>. *J. Chem. Phys.* **153**. 034706. 10.1063/5.0012721 (2020).
- [68] M. Braun and O. I. Kartavtsev, Faddeev calculations for thr three-electron quantum dot. *Nucl. Phys. A* **698**, 519c (2001).
- [69] M. Braun and O. I. Kartavtsev, Lowest energy states of three identical charged particles in a two-dimensional harmonic trap. *Phys. Lett. A* **331**, 437 (2004).
- [70] N. S. Rytova, Screened potential of a point charge in a thin film. *Proc. MSU Phys., Astron.* **3**, 30 (1967), <https://www.researchgate.net/publication/320224883>
- [71] L. V. Keldysh, Coulomb interaction in thin semiconductor and semimetal films. *JETP Lett.* **29**, 658 (1979).
- [72] P. Cudazzo, I. V. Tokatly, and A. Rubio, Dielectric screening in two-dimensional insulators: implications for excitonic and impurity states in graphene. *Phys. Rev. B* **84**, 085406 (2011).
- [73] I. S. Gradshteyn and I. M. Ryzhik, *Table of Integrals, Series, and Products*, 7th Edition, Elsevier, Amsterdam 2007.
- [74] *Handbook of Mathematical Functions with Formulas, Graphs, and Mathematical Tables*, edited by M. Abramowitz and I. A. Stegun, NBS Applied Mathematics Series 55, National Bureau of Standards, Washington, 1964.
- [75] L. D. Faddeev and S. P. Merkuriev, *Quantum Scattering Theory for Several Particle Systems* (Kluwer Academic, Dordrecht, 1993) pp. 398.
- [76] I. Filikhin, R. Ya. Kezerashvili, and B. Vlahovic, The charge and mass symmetry breaking in the  $KK\bar{K}$  system. *J. Phys. G: Nucl. Part. Phys.* **51** (2024), in press <https://doi.org/10.1088/1361-6471/ad133c>
- [77] D. Xiao, G-B. Liu, W. Feng, X. Xu, and W. Yao, Coupled spin and valley physics in monolayers of MoS<sub>2</sub> and other group-VI dichalcogenides. *Phys. Rev. Lett.* **108**, 196802 (2012).
- [78] R. I. Jibuti and K. V. Shitikova, *Method of hyperspherical functions in atomic and nuclear physics*. Energoatomizdat, Moscow, 270p. 1993. (in Russian).
- [79] J. Avery, *Hyperspherical Harmonics; Applications in Quantum Theory*, Kluwer Academic Publishers, Dordrecht, 1989.
- [80] J. Avery, *Hyperspherical Harmonics and Generalized Sturmians*. Progress in Theoretical Chemistry and Physics, Kluwer Academic Publishers, New York, 2002.
- [81] J. E. Avery and J. S. Avery, *Hyperspherical Harmonics and Their Applications*, World Scientific, London, 2018.
- [82] J. Raynal and J. Revai, Transformation coefficients in the hyperspherical approach to the three-body problem. *Nuovo Cim.* **68A**, 612 (1970).
- [83] Landau, L. D. & Lifshitz, E. M. *Quantum Mechanics: Non-Relativistic Theory* (Pergamon, Oxford, 1977).
- [84] B. Zaslav and M. E. Zandler, Two-dimensional analog of the hydrogen atom. *Am. J. Phys.* **35**, 1118 (1967).
- [85] X. L. Yang, S. H. Guo, F. T. Chan, K. W. Wong, and W. Y. Ching, Analytical solution of a two-dimensional hydrogen atom. I. Nonrelativistic theory. *Phys. Rev. A* **43**, 1186 (1991).
- [86] D. G. W. Parfitt and M. E. Portnoi, The two-dimensional hydrogen atom revisited. *J. Mat. Phys.* **43**, 4681 (2002).
- [87] R. Ya. Kezerashvili, J. Luo, and C. R. Malvino, On an exactly solvable two-body problem in two-dimensional quantum mechanics. *Few-Body Syst.* **64**, 79 (2023).
- [88] F. Gesztesy and L. Pittner, Electrons in logarithmic potentials I. Solution of the Schrodinger equation. *J. Phys. A: Math. Gen.* **11**, 679 (1978).
- [89] H. J. W. Müller-Kirsten and S. K. Bose, Solution of the wave equation for the logarithmic potential with application to particle spectroscopy. *J. Math. Phys.* **20**, 2471 (1979).
- [90] A. A. Khelashvili, V. Yu. Khmaladze, and N. D. Chachava, Many-body problem with logarithmic potentials and its application to the quarks bound states. *Teor. Mat. Fiz.*, **62**, 136 (1985).
- [91] H. F. Weber, Ueber die Integration der partiellen Differentialgleichung  $\partial^2 u / \partial x^2 + \partial^2 u / \partial y^2 + k^2 u = 0$ . *Math. Ann.*, **1**, 1-36 (1869).
- [92] C. Robert, T. Amand, F. Cadiz, D. Lagarde, E. Courtade, M. Manca, T. Taniguchi, K. Watanabe, B. Urbaszek, and X. Marie, Fine structure and lifetime of dark excitons in transition metal dichalcogenide monolayers, *Phys. Rev. B* **96**, 155423 (2017).
- [93] K. F. Mak, K. He, J. Shan, and T. F. Heinz, Control of valley polarization in monolayer MoS<sub>2</sub> by optical helicity. *Nat. Nanotechnol.* **7**, 494 (2012).
- [94] T. Cao, G. Wang, W. Han, H. Ye, C. Zhu, J. Shi, Q. Niu, P. Tan, E. Wang, B. Liu et al., Valley-selective circular dichroism of monolayer molybdenum disulphide. *Nat. Commun.* **3**, 887 (2012).
- [95] H. Zeng, J. Dai, W. Yao, D. Xiao, and X. Cui, *Nat. Nanotechnol.* **7**, 490 (2012).

- [96] G. Sallen, L. Bouet, X. Marie, G. Wang, C. R. Zhu, W. P. Han, Y. Lu, P. H. Tan, T. Amand, B. L. Liu et al., *Phys. Rev. B* **86**, 081301 (2012).
- [97] G. Wang, E. Palleau, T. Amand, S. Tongay, X. Marie, and B. Urbaszek, Polarization and time-resolved photoluminescence spectroscopy of excitons in MoSe<sub>2</sub> monolayers. *Appl. Phys. Lett.* **106**, 112101 (2015).
- [98] D. MacNeill, C. Heikes, K.-F. Mak, et al., Breaking of valley degeneracy by magnetic field in monolayer MoSe<sub>2</sub>. *Phys. Rev. Lett.* **114**, 037401 (2015).
- [99] F. Gao, Y. Gong, M. Titze, et al., Valley trion dynamics in monolayer MoSe<sub>2</sub>. *Phys. Rev. B* **94**, 245413 (2016).
- [100] T. Yan, J. Ye, X. Qiao, P. Tan, and X. Zhanga, Exciton valley dynamics in monolayer WSe<sub>2</sub> probed by the two-color ultrafast Kerr rotation. *Phys. Chem. Chem Phys.* **4**, 2599 (2017).
- [101] J. Huang, T. B. Hoang, T. Ming, J. Kong, and M. H. Mikkelsen. Temporal and spatial valley dynamics in two-dimensional semiconductors probed via Kerr rotation. *Phys. Rev. B* **95**, 075428 (2017).
- [102] K. Hao et al., Trion valley coherence in monolayer semiconductors. *2D Mater.* **4**, 025105 (2017).
- [103] X.-X. Zhang, T. Cao, Z. Lu, Y.-C. Lin, F. Zhang, Y. Wang, et al., Magnetic brightening and control of dark excitons in monolayer WSe<sub>2</sub>. *Nat. Nanotechnol.* **12**, 883 (2017).
- [104] T. Cheiwchanamngij and W. R. L. Lambrecht, Quasiparticle band structure calculation of monolayer, bilayer, and bulk MoS<sub>2</sub>. *Phys. Rev. B* **85**, 205302 (2012).
- [105] A. Ramasubramaniam, Large excitonic effects in monolayers of molybdenum and tungsten dichalcogenides. *Phys. Rev. B* **86**, 115409 (2012).
- [106] A. F. Nikiforov and V. B. Uvarov, *Special Functions of Mathematical Physics. A Unified Introduction with Applications.* Springer Basel AG, 1988.
- [107] M. R. Molas, A. Slobodeniuk, K. Nogajewski, M. Bartos, L. Bala, et al., Energy spectrum of two-dimensional excitons in a nonuniform dielectric medium. *Phys. Rev. Lett.* **123**, 136801 (2019).
- [108] S. Latini, T. Olsen, and K. S. Thygesen, Excitons in van der Waals heterostructures: The important role of dielectric screening. *Phys. Rev. B* **92**, 245123 (2015).
- [109] K. Andersen, S. Latini, and K. S. Thygesen, Dielectric genome of van der Waals heterostructures. *Nano Lett.* **15**, 4616 (2015).
- [110] D. V. Tuan, M. Yang, and H. Dery, Coulomb interaction in monolayer transition-metal dichalcogenides, *Phys. Rev. B* **98**, 125308 (2018).
- [111] A. M. Jones, H. Yu, J. Schaibley, J. Yan, D. G. Mandrus, T. Taniguchi, K. Watanabe, H. Dery, W. Yao, and X. Xu, Excitonic Luminescence upconversion in a two-dimensional semiconductor, *Nat. Phys.* **12**, 323 (2016).
- [112] H. Dery and Y. Song, Polarization analysis of excitons in monolayer and bilayer transition-metal dichalcogenides, *Phys. Rev. B* **92**, 125431 (2015).